HHS Public Access

Author manuscript

Circ Res. Author manuscript; available in PMC 2022 September 17.

Published in final edited form as:

Circ Res. 2021 September 17; 129(7): e121–e140. doi:10.1161/CIRCRESAHA.121.318897.

Circulating Pro-inflammatory Exosomes Worsen Stroke Outcomes in Aging

Hongxia Zhang, **Siyang Lin**, **Christopher L. McElroy**, **Brian Wang**, **Dana Jin**, **Victor V. Uteshev**, **Kunlin Jin**

Department of Parmacology and Neuroscience, University of North Texas Health Science Center, Fort Worth, TX 76107, USA

Abstract

Rationale: The systemic inflammatory milieu plays an important role in the age-related decline in functional integrity, but its contribution to age-related disease (e.g., stroke) remains largely unknown.

Objective: To determine the role of systemic inflammatory milieu in ischemic stroke.

Methods and Results: Here, we report that systemic administration of serum exosomes from young rats (Y-exo) into aged ischemic rats improved short- and long-term functional outcomes after ischemic stroke and reduced synaptic loss. By contract, similar injections of serum exosomes from aged rats (O-exo) into aged ischemic rats worsened sensorimotor deficits through exacerbation of synaptic dysfunction due to excessive microglial phagoptosis (primary phagocytosis). Our proteomic analysis further revealed that the expression of CD46, a C3b/C4b-inactivating factor, was higher in Y-exo, compared to O-exo. Whereas the prevalence of pro-inflammatory mediators (C1q, C3a and C3b) in serum exosomes increased with age. Microglial expression of C3a/b and C3aR increased after O-exo treatment, compared with Y-exo and vehicle groups. Administration of a selective C3aR inhibitor or microglial depletion attenuated synaptic dysfunction associated with O-exo treatment and improved post-stroke functional recovery.

Conclusion: Our data suggest that the levels of pro-inflammatory mediators in serum exosomes increase with age and are associated with worsened stroke outcomes through excessive C3aR-

Address Correspondence to: Dr. Kunlin Jin, Professor, Department of Pharmacology and Neuroscience, University of North Texas Health Science Center at Fort Worth, Fort Worth, TX 76107, USA, Tel: 817-7352579, kunlin.jin@unthsc.edu.

AUTHOR CONTRIBUTIONS

H.Z. and K.J. conceived the project. H.Z., S. Y., V. V. U., D.J. and C.L.M. performed the experiments. H.Z. performed ischemic stroke model. H.Z., S.Y., and B.W. performed tissue immunofluorescence staining and Western blotting. H.Z and C.L.M. performed Golgi staining and analysis. H.Z. performed bioinformatic analyses. H.Z. S.Y. and D.J. performed blinded histology scoring, brain sections and neurobehavioral tests. V.V. U. performed whole-cell patch clamp, electrophysiological data analysis and edited the revised draft. K.J. assisted with experiments. H.Z., B.W., and K.J. wrote the manuscript.

DISCLOSURES

None.

SUPPLEMENTAL MATERIALS

Online Figures I-VIII

Online Table I

Major Resource Table

dependent microglial phagoptosis. Modulation of this process may serve as a promising therapy for stroke and other age-related brain disorders.

Graphical Abstract

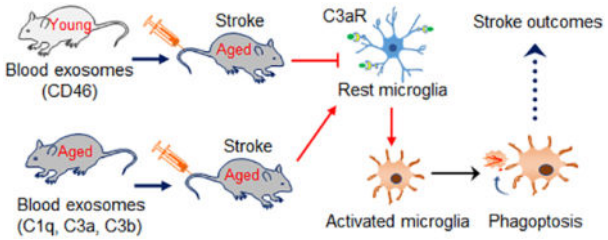

Circulating exosomes could act as a neuroinflammatory mediators in systemic inflammation and contribute to age-related decline in functional integrity. However, their role in ischemic stroke remains unexplored. In this study, we found that aging blood exosomes progressively accumulate peripheral pro-inflammatory mediators and could cross the BBB to prime and excessively activate microglia via a C3aR-dependent mechanism. This process is facilitated by ischemic stroke resulting in synaptic damage, reduced synaptic function, and elevated sensorimotor and cognitive deficits. By replacing aging exosomes with young exosomes, it is possible to reverse the decline of synaptic and neurological functions and deliver therapeutic benefits after stroke. Thus, the peripheral and central immune systems are engaged in a continuous crosstalk via complement-microglial interactions and their modulation may serve as a promising therapeutic tool in ischemic stroke and other age-related brain diseases.

Subject Terms:

Inflammation; Ischemia; Mechanisms; Translational Studies

INTRODUCTION

Aging is a fundamental biological process accompanied by a general decline in tissue function, increased susceptibility to neurological disorders and reduced resistance to inflammation and infection. Age-related sensorimotor and neurocognitive decline in the elderly is becoming a health care priority in the United States and around the world.[1] Despite tremendous public support and financial investments, the search for clinically effective therapeutic strategies that may help to delay or decelerate the aging process and associated age-related disorders remains a considerable challenge. Ischemic stroke is one of these disorders and remains the fifth leading cause of death and the leading cause of long-term disability in the United States with limited treatment options. Although the underlying mechanisms of aging remain elusive, attempts to revitalize to the aging systemic milieu by introducing new blood to old organisms have produced promising results. Compelling evidence indicates that systemic administration of young blood plasma into aged mice reverses age-related cognitive decline,[2] whereas exposing young mice to plasma from aged mice impairs their cognitive function.[3] Similarly, age-related decline in myogenesis and neurogenesis can be restored after exposure to a “youthful” systemic environment through heterochronic parabiosis.[4, 5] Importantly, age-related cardiac hypertrophy can also

be reversed by exposure to a young systemic environment also resulting in reduced cardiomyocyte size[6]. Currently, there is little evidence for a direct association of age-related diseases such as ischemic stroke with age-related changes in blood exosomes.

Exosomes are extracellular microvesicles that contain specific proteins, RNA, microRNAs (miRNAs) and long noncoding RNAs (lncRNAs)[7]. Although exosomes were discovered several decades ago,[8] only recently have they been shown to be vital in cell communication by transferring their cargo between source and target cells, through which they can affect the rate of aging,[9] the development and progression of cardiovascular disease[10] and cancer.[11] Pusic *et al.*[12] found that the youthful systemic milieu enhances remyelination in aged animals and that environmental enrichment of aged animals produces exosomes that mimic this promyelinating effect.[13] Consistent with these results, recent studies have shown that administration of exosomes released from mesenchymal stromal cells promotes neuroplasticity and functional recovery after ischemic stroke.[14, 15] Based on these findings, we hypothesized that peripheral circulating exosomes derived from young or aged animals may serve as vehicles to deliver beneficial or detrimental signals, respectively, from the periphery to the brain and may thus influence functional outcomes after ischemic stroke.

In this study, we found that systemic administration of serum exosomes from aged rats (O-exo) into aged ischemic rats worsened sensorimotor deficits, increased infarct volume, primed the microglial phagoptosis (primary phagocytosis) and increased synaptic loss. Conversely, exposing aged rats to serum exosomes from young rats (Y-exo) supported synaptic plasticity and improved short- and long-term functional outcomes after ischemic stroke. Through proteomic analysis, we found that pro-inflammatory mediators (C1q, C3a and C3b) in serum exosomes increases whereas exosomal level of CD46, a C3b/C4b-inactivating factor, decreases with age. Microglial expression of C3a, C3b and C3a receptor (C3aR) increased after O-exo treatment. Inhibition of C3aR or microglial depletion attenuated synaptic loss and sensorimotor deficits associated with O-exo treatment. These data suggest that O-exo act as brain-permeable inflammatory mediators able to define the outcome of ischemic stroke in aged rats by priming C3aR-dependent microglial phagoptosis.

METHODS

Data Availability.

The experimental data supporting this study's findings are available from the corresponding author upon request.

Focal Ischemic Stroke.

Young (3-month-old) and aged (21- to 23-month-old) male Fisher 344 rats were obtained from the National Institute of Aging (NIA) aged rodent colonies. All experiments were performed with male rats, as ovarian sex hormones in female rats significantly impact the functional outcome after ischemic stroke.[16] Rats were anesthetized with 2.0% isoflurane in 70% N_2O/30% O_2 using a mask. Permanent distal middle cerebral artery occlusion (dMCAO) with or without bilateral CCA occlusion, was performed as described previously to determine the mortality rate after dMCAO.[17] Permanent dMCAO model without

occlusion of common carotid artery (CCA) was applied to all experiments in this study. Briefly, a 2-cm incision was made between the left eye orbit and tragus under the surgical microscope. The temporal muscle was retracted laterally, and a 3-mm diameter craniotomy was made rostral to the foramen ovale. The dura was incised with a 26–gauge needle and the distal middle cerebral artery (MCA) was exposed. The left MCA was occluded by electrocoagulation (Fine Science Tools, Cat# 18000-00) without damaging the brain surface. Interruption of blood flow was confirmed visually under the microscope, the temporal muscle was repositioned, and the skin was closed. Rectal temperature was measured and maintained at 37 ± 0.2°C with a heating blanket (Harvard Apparatus, Cat # 507220F). In sham-operated controls the distal MCA was visualized but not occluded. All animal procedures were approved by Institutional Animal Care and Use Committee (IACUC) of University of North Texas Health Science Center and conducted according to the National Institutes of Health (NIH) Guide for the Care and Use of Laboratory Animals. Every effort was made to minimize suffering and to reduce the number of animals used.

Isolation of Serum Exosomes.

Whole blood was collected from young or aged rats *via* cardiac puncture into a BD Vacutainer® Plus Glass Serum blood collection tubes (BD, Cat# 366430). After collection, the whole blood samples were allowed to clot at room temperature for 30 min. The clots were removed by centrifugation for 10 min at 1,000 × *g* using a refrigerated centrifuge. The isolated serum was aliquoted and stored at −80°C.

Exosomes from young or aged rat serum were isolated using the ExoQuick Exosome precipitation kit (System Biosciences, Cat# EXOQ20A-1) according to the manufacturer's instructions. In brief, serum (500 μl) was centrifuged at 3000 × *g* for 15 min to eliminate cells and cell debris. The supernatant was transferred to a sterile microtube and an appropriate volume of exosome precipitation solution was added for 30 min at 4°C. The mixture was then centrifuged at 1500 × *g* for 30 min, and the exosome pellet was resuspended in sterile phosphate-buffered saline (PBS), aliquoted and stored at −80 ° or used immediately for experiments.

Injection of Serum Exosomes.

The rats were anesthetized as described above and the lateral tail vein was dilated by immersion in warm water. Serum exosomes (300 μg in 200 μl) from young or aged male Fisher 344 rats or vehicle (PBS) were injected into the lateral tail vein of young or aged male rats 3 h or 6 h after dMCAO, twice per day for 3 days. Rats were euthanized at different durations after injection, and the brains were sampled.

To monitor peripheral circulating exosomes trafficking in the brain, the exosomes were labeled with the ExoGlow-Vivo dye, a unique dye developed for *in vivo* studies, using the ExoGlow-Vivo EV Labeling Kit (System Biosciences, Cat# EXOGV900A-1). The labeled exosomes or vehicle were administered intravenously via the lateral tail vein into sham-operated or ischemic rats 3 h after dMCAO. The rats were then euthanized 1, 3, 7, 14 and 21 days after injection.

Characterization of Serum Exosomes.

The concentration and size distribution profile of isolated exosomes were determined by nanoparticle-tracking analysis (NTA) using SBI's Exosome Nanosight Analysis Service (System Biosciences, Palo Alto, CA). The serum exosomes were also observed using transmission electron microscopy (TEM, FEI Tecnai G2 Spirit BioTwin) to identify the morphology and the extent of dispersion, which was performed at the Electron Microscopy Core Facility, University of Texas Southwestern Medical Center, Texas, USA. The enrichment of exosomes was further confirmed by Western blot using antibodies against exosomes, such as CD63, CD9, and CD81.

Infarct Volume Measurement.

Infarct volume was determined as described previously.[18, 19] Rats were anesthetized with 4% isoflurane in 70% N_2O and 30% O_2 and decapitated after treatment. The brains were removed quickly and cut into 2-mm sections. The sections were stained with 2% 2,3,5-triphenyltetrazolium chloride (TTC; Sigma-Aldrich, St. Louis, MO, USA. Cat# T8877) solution for 10 min at 37°C and then fixed in 4% paraformaldehyde (PFA) solution in PBS overnight. Rat brains were also cut into 5-μm (paraffin-embedded tissue) or 30-μm (frozen tissue) coronal sections and stained with 0.1% Cresyl violet (CV; Sigma-Aldrich, St. Louis, MO, USA. Cat# C5042). Both stained sections were photographed using a Nikon E 950 digital camera attached to a dissecting microscope, and infarct area was measured using NIH's Image J (version 1.62; https://imagej.nih.gov/ij/). The ischemic area was calculated as the difference between the intact area of contralateral hemisphere and the intact area of the ischemic hemisphere. Edema-adjusted (E_A)-infarct volume was calculated by multiplying the infarct area by the thickness of the section and expressed as a percentage of the intact contralateral hemispheric volume as described previously.[18]

Measurement of BBB Disruption.

To determine the permeability of the cerebral vasculature, rats were intravenously injected via the lateral tail vein with 2% Evans Blue (EB; Sigma-Aldrich, Cat# E2129) in 1 X PBS (4 mL/kg of body weight) 1 h or 23 h after onset of dMCAO. The rats were euthanized 24 h after dMCAO, and then perfused with ice-cold PBS. Brains were removed, cut into 2-mm slices, and the affected regions were identified by TTC + EB co-staining.

Golgi-Cox Staining.

Golgi-Cox staining was performed to visualize dendritic spine structure in superficial and deep cortical layer neurons using the FD Rapid GolgiStain kit (FD Neuro-technologies, Inc, Cat # PK401/401A) according to the manufacturer's instruction.[20, 21] In brief, rats were deeply anesthetized and intracardially perfused with PBS, followed by 4% PFA. The brain sections were immersed in the Golgi-Cox solution for 12 days in the dark at room temperature and then transferred to 30% sucrose solution. Coronal sections were cut at 60-μm and stained according to FD Rapid GolgiStain's protocol. The slides were subsequently washed with distilled water followed by dehydration in ascending alcohol concentrations, cleared in xylene, and then mounted with Per-mount (Vector Labs, H-5000).

Quantification of Dendrites and Dendritic Spines.

Dendrites and dendritic spines were analyzed from cortical layers II/III or V of the ischemic penumbra (peri-infarct) primary motor cortex (M1) between 0 and 0.5 mm anterior to the bregma, corresponding to the approximate center of the cortical infarct, with the aid of an atlas.[22] M1 regions were chosen as previous study showed that focal ischemic stroke induced significant structural plasticity in the penumbra motor cortex but not in the more distant ipsilateral cortical regions.[23] In addition, dendrite and dendritic spine structure was also examined in the M1 region of the contralateral cortex (same animal as control). Criteria for inclusion in the analyses were that the neuron had to be well impregnated with Golgi-Cox stain, unobstructed by other dendrites, blood vessels or glia, and that the dendritic arborization was intact and visible in the plane of the section.

Three images of the penumbral M1 region of the ischemic brain per section or the corresponding region on the contralateral cortex were captured by using an Olympus confocal scanning system mounted on Olympus microscope (BX 61, Olympus) with an HSD channel and FV 10-ASW software (Olympus Fluoview, Version 4.02). Dendrites and dendritic spines were analyzed in at least 9 randomly selected pyramidal cells in the penumbra per animal and at least 4 animals per condition/group. The mean of all neurons in each individual animal was used for statistical comparison between conditions. As a result, the mean number of dendrites and dendritic spines per neuron was evaluated for each animal. These numbers were then averaged across animals of the same condition/group and differences across conditions/groups were statistically analyzed. For quantification of dendrites and spines of pyramidal neurons, NIH's image J (version 1.62) was used to invert image signals to RGB. Imaris software (version 8.0, Bitplane) was used to track neurites with the FilamentTracer module by means of a semiautomatic autopath method. Fifty images were collected as high-resolution image z-stacks with a step size of 0.66 μm. On the semiautomatically tracked dendrites, Golgi stains were manually indicated under interactive 3D visualization using the built-in Spot detection module. Staining in each dendritic segment underwent manual thresholding such that all visually discernible protuberances in 3D were identified according to the range values of the length of spines in the cortical M1 region. Both apical and basilar dendritic trees were analyzed for total length and total number of spine segments.[24] The length and diameter of dendritic spines were automanually marked in each individual dendritic spine from the center of the dendritic shaft to the distal tip of the spine based on a threshold. Dendritic length and branches were determined by a measure of the total length of each basal or apical dendrite and the number of dendritic spines refers to all dendritic spines contained within the total length of each dendrite. The same measurement paradigm was applied to all neurons tested.

Whole-cell Patch-clamp Recordings.

Three-four coronal whole-brain slices (280 μm thickness) containing the ischemic penumbra were cut in a sucrose-rich solution at 3°C using a 7000smz-2 vibrating microtome (Campden Instruments Ltd., Lafayette, IN, USA). The sucrose-rich solution was of the following composition (in mM): 250 sucrose, 3 KCl, 1.23 NaH_2PO4, 5 $MgCl_2$, 0.5 $CaCl_2$, 26 $NaHCO_3$ and 10 glucose (pH 7.4, when bubbled with carbogen, i.e., 95 % O_2 and 5% CO_2). The brain slices were then transferred to a temporary storage chamber where they were maintained

at 30°C for ~1 h and then, up to 8 h at room temperature in an oxygenated artificial cerebrospinal solution (ACSF) of the following composition (in mM): 125 NaCl, 3 KCl, 1.23 NaH_2PO_4, 1 $MgCl_2$, 2 $CaCl_2$, 26 $NaHCO_3$ and 10 glucose (pH 7.4, when bubbled with carbogen).

For patch-clamp recordings, slices were transferred to a recording chamber perfused with ACSF at room temperature. Recordings were made using a MultiClamp-700B amplifier and Digidata-1440A A/D converter (Molecular Devices, Sunnyvale, CA, USA). Data were sampled at 10 kHz and filtered at 2 kHz. A concentric stimulation electrode (FHC, Bowdoin, ME, USA) was connected to a GRASS S88 stimulator and used to stimulate presynaptic terminals in the cortical layer I to cause neurotransmitter release in the cortical layer III where the recording neurons were located. In each experiment, 50 pairs of identical brief electrical stimuli (~4 ms, ~0.8 mA, every 15 s) separated by 250 ms were given and ePSCs were recorded, averaged and analyzed offline. Recording pipettes were pulled using a Sutter P-97 puller (Sutter Instruments, Novato, CA, USA). The pipette resistance was 4–6 MΩ when filled with a K-gluconate-based internal solution. After formation of a giga-seal (>2 GΩ), the whole-cell configuration was established. Recordings were conducted at room temperature. The membrane voltage was clamped at −70 (±5) mV. The extracellular solution was identical to ACSF that was used for preparation and storage of slices. The recording electrodes were filled with an intracellular solution of the following composition (in mM): 140 K-gluconate, 1 NaCl, 2 $MgCl_2$, 2 Mg-ATP, 0.3 Na-GTP, 10 HEPES (pH 7.4 adjusted with KOH). The membrane voltage was not corrected for the liquid junction potential: V_{LJ}~16 mV. A custom-made perfusion pump was used to perfuse slices in the recording chamber at a rate of 2 ml/min.

Immunohistochemistry and Immunofluorescence Staining.

Immunohistochemistry and double or triple immunofluorescence staining were performed on brain sections as previously described.[25, 26] The primary antibodies used were as follows: rabbit anti-Iba1 (1:1000, WAKO, Cat# 019-19741), chicken anti-Homer1 (1:500, Synaptic Systems, Cat# 160006), mouse anti-CD68 (1:100, Serotec, Cat# MCA341R), rabbit anti-CD68 (1:200, ThermoFisher Scientific, Cat # PA5-78996), goat anti-CD86 (1:200, R&D, Cat# AF1340), rat anti-CD206 (1:100, Serotec, Cat# MCA2235GA), rabbit anti-NeuN (1: 100, Millipore, Cat# ABN78) and rabbit anti-GFAP (1: 500, DAKO, Cat # Z0334), mouse anti-C3aR (1: 50, Santa Cruz, Cat# sc-133172), rabbit anti-Von Willebrand Factor (vWF;1: 100, Millipore, Cat# AB7356), goat anti-MPO (1:70, R&D, Cat# AF3667-SP), goat anti-CD45 (1:50), R&D, Cat# AF114-SP) and Mouse anti-CD11b (OX-42; 1:500, Bio-Rad, Cat# MCA275R). The secondary antibodies used were as follows: Alexa Fluor 350-, 488-, 594-, or 647-conjugated donkey anti-rat, anti-rabbit, anti-mouse, anti-chicken, or anti-goat IgG (1:1,000, ThermoFisher Scientific) and horse biotinylated antibody (1:200, Vector Laboratories, Cat# BA-9500). DAPI (4′,6-diamidine-2-phenylindole dihydrochloride; Vector Laboratories) was used to counterstain nuclei, and fluorescence signals were detected with Olympus confocal scanning microscope.

For co-localization analysis, double or triple immunostained-positive cells in the penumbra were imaged with X60 Zeiss Neofluar oil-immersion objective (numerical aperture=1.3)

using sequential scanning mode. Corresponding images were taken in the contralateral cortex. Three standard sections with 9 fields per animal in 200-μm intervals were analyzed. A secondary antibody only control was used in immunohistochemistry and immunofluorescence staining. All sections were scanned with the same acquisition parameters.

Western Blot.

The different brain regions were dissected, and brain tissue was lysed in RIPA buffer (1% Triton-X100, 0.5% sodium deoxycholate, 0.1% SDS in 1X PBS, pH 7.4) with 1X protease and phosphatase inhibitor cocktail (ThermoFisher Scientific, Cat# 78440). The protein concentration was determined using Quick Start Bradford protein assay (Pierce™ BCA Protein Assay kit, Thermo Fisher Scientific) and normalized for protein content. The lysates (30 μg) were loaded on 8–12% SDS-PAGE gels and subsequently transferred onto a polyvinylidene difluoride (PVDF) membrane (Merck Millipore, Cat# IPVH00010). The blot was incubated in blocking buffer (5% milk in Tris-buffered saline with 0.1% Tween 20) and then incubated with the primary antibody solution overnight at 4°C. Protein signals were detected with horseradish peroxidase–conjugated secondary antibodies and Pierce enhanced chemiluminescence (ECL) substrate (ThermoScientific, Cat# 32106). The data were recorded and analyzed using the ChemiDoc Imaging System (Bio-Rad). β-actin was used for normalization for tissue samples and C9 was used for normalization for exosomes samples.

Primary antibodies include mouse anti-CD63 (1:1000, BD Pharmingen, Cat # 551458), mouse anti-CD9 (1:1000, BD Pharmingen, Cat# 551808) and mouse anti-CD81 (1:1000, Santa Cruz, Cat #sc-7637), rabbit anti-Iba1 (1:2000, WAKO, Cat# 019-19741), mouse anti-CD68 (1:1000, Serotec, Cat# MCA341R), mouse anti-C3 (1:100, Santa Cruz, Cat# sc-28294), rat anti-CD46 (1:100, Abcam Cat# ab180625), mouse anti-C1q (1:100, Abcam, Cat# ab71940), mouse anti-β-actin (1:2000, Cell Signaling Tech, Cat# 3700s), goat anti-CD86 (1:200, R&D, Cat# AF1340), mouse anti-C3aR (1: 100, Santa Cruz, Cat# sc-133172), mouse anti-CD11b (1:100, Serotec; Cat# MCA275R), rat anti-CD206 (1:100, Serotec, Cat# MCA2235GA). Secondary antibodies include horseradish peroxidase (HRP)-conjugated anti-rabbit, anti-mouse, anti-rat, anti-goat IgG secondary antibodies (Cell Signaling Tech).

Multiplex analysis of Cytokines and Chemokines.

To investigate the effect of serum exosomes on the systemic inflammatory status, the levels of 27 cytokines/ chemokines in the serum of aged ischemic rats were simultaneously quantified 72 h after Y-exo or O-exo treatment by using the Rat Cytokine Array/Chemokine Array 27-Plex (Eve Technologies Corp, Calgary, AB, Canada). The assay was performed at Eve Technologies by using the Bio-Plex™ 200 system (Bio-Rad Laboratories, Inc., Hercules, CA, USA) according to their protocol. The 27-Plex consisted of EGF, Eotaxin, Fractalkine, G-CSF, GMCSF, GRO/KC/CINC-1, IFNγ, IL-1α, IL-1β, IL-2, IL-4, IL-5, IL-6, IL-10, IL-12(p70), IL-13, IL-17A, IL-18, IP-10, Leptin, LIX, MCP-1, MIP-1α, MIP-2, RANTES, TNFα and VEGF.

Proteomic Analysis.

Exosomes isolated from young and aged rat blood were processed for proteomic analysis by SBI's Exosome Proteomics Services (System Biosciences, USA). The protein concentration of each exosome was determined by Qubit fluorometry (Invitrogen) and each sample (10 μg) was processed by 10% SDS-PAGE. The band was excised, and in-gel digestion was performed using a ProGest robot (DigiLab). The different proteomic contents of Y-exo and O-exo were analyzed using nano liquid chromatography tandem mass spectrometry (LC-MS/MS) with a Waters NanoAcquity HPLC system interfaced to a ThermoFisher Q Exactive. The resulting LC-MS/MS raw data were processed using Mascot (Matrix Science) and searched against the UniProt Rat database. The Mascot DAT files were parsed into Scaffold (Proteome Software) for validation, filtering and to create a non-redundant list per sample. Data were filtered using 1% protein and peptide false discovery rate (FDR) and requiring at least two unique peptides per protein. The criteria for protein identifications were accepted if a minimum of two peptides were detected or a unique peptide was detected with an FDR <1%.

Biological Functions and Pathway Analysis.

Biological function annotation of the proteins was analyzed by Blastp (Blast2GO version 4) using whole database, and mapped, annotated with gene ontology (GO) database (http://geneontology.org/). Hierarchical cluster analysis (HCA) is an algorithmic approach to identify groups with varying degrees of (dis)similarity in a data set represented by a (dis)similarity matrix. This analysis was carried out with the Pheatmap package (https://CRAN.R-project.org/package=pheatmap, Estonia). The volcano plot is a type of scatter-plot that can quickly identify changes in individual data in large data-sets composed of replicate data; ggplot2 package (http://ggplot2.org, New Zealand) was used for this purpose. All of the rat proteins were used as the basis for calculating enrichment values. Statistically altered functions of different expressed exosome proteins were calculated by Fisher's exact test in Blast2GO. A cutoff of absolute fold change ≥ 1.5 was used for differentially expressed proteins and a corrected p - value < 0.05 was considered significant.

C3aR Antagonist Treatment.

SB290157 (Cat# 559410, Merck Millipore), a C3aR inhibitor,[27] was diluted in sterile PBS/0.5% DMSO to a concentration of 1 nM, as previously described.[28] Ischemic rats were randomized to receive intraperitoneal injections of either SB290157 (1 mg/kg) or an equal volume of vehicle (PBS/DMSO) 1 h prior to exosome administration. Outcome was determined 72 h after treatment.

Microglial Depletion.

To deplete microglia *in vivo*, rats were fed with the colony stimulating factor 1 receptor (CSF1R) inhibitor PLX3397 (MedChemExpress Inc. Cat# HY-16749) formulated in standard chow (Lab Diet 5LG4, Lab Supply Inc.) at 290 mg/kg as previously described.[29] Respective controls received standard chow. Rats were fed for at least 28 days prior to dMCAO to ensure maximum microglia depletion, which was maintained until the end of the experiment.

Neurobehavioral Tests.

Rats underwent neurobehavioral tests to evaluate sensorimotor and cognitive function. Animals were trained prior to ischemic stroke and sensorimotor and cognitive deficit were assessed at different durations thereafter. The investigators performing the tests were blinded to group and treatment allocation.

The skilled ladder rung walking test was used to evaluate placing, stepping and inter-limb coordination[30] and the procedure was performed as described previously.[31] Animals were video recorded as they walked across the runway five times per session. Missteps were evaluated using a 6-point grading scale according to the precision of limb placement on the rungs: 0 total miss, 1 deep slip, 2 slight slip, 3 replacements, 4 corrections, 5 partial placements, 6 correct placements. Scores 0–2 were defined as errors. The percentage of errors in total steps was calculated and averaged over five trials for each rat. Cylinder test was performed to assess spontaneous forelimb use as described previously.[32] The 28-point neuroscore test was used to evaluate sensorimotor function with modification from methods previously described.[33] The Morris Water Maze (MWM) test was used to assess spatial learning and long-term memory to investigate the post-stroke cognitive impairment as previously described.[34]

Statistical Analysis.

All values were expressed as mean ± SEM. The sample size and P values are provided with each figure. All experiments were randomized and performed by a researcher blinded to group and treatment allocation. The data normality was determined using a Shapiro-Wilks test. For normally distributed populations of data points, a Student *t*-test (2 groups) or a one-way ANOVA followed by a Tukey post-hoc test (>2 groups) were used. For data that failed the normality test, a Mann-Whitney test (2 groups), or a Kruskal-Wallis test with a Dunn post-test (>2 groups) were used. One limitation of this analysis is that it did not correct for multiple testing across the whole study. Values of $p < 0.05$ were considered statistically significant. All statistical analyses were conducted using a GraphPad Prism software (version 8.02; GraphPad Software, San Diego, CA; https://www.graphpad.com). We only excluded animals that died or with an apparent failure of TTC staining. The sample size and the number of animals were estimated from the power analysis existing studies with the anticipated effects size =30%, α=0.05 and (1-β) = 0.8 using a SYSTAT-13 software (https://systatsoftware.com/products/systat/). The statistical analysis in the animal experiments was done on the basis of at least three independent experiments. Representative images were selected to most accurately represent the group mean/average across all the available data.

RESULTS

Age-related Changes in Characteristics of Serum Exosomes.

To investigate whether age-dependent peripheral circulating exosomes could act as inflammatory mediators to influence functional outcome after ischemic stroke, we isolated serum exosomes from 3-month-old (Y-exo) and 21- to 23-month-old (O-exo) rats, which correlate to ~20 and 56–69 years of age in humans, respectively. We first performed

Western blot with antibodies against exosome-specific markers to confirm the enrichment of exosomes (Figure 1A). We also verified serum exosome morphology and size using transmission electron microscopy (TEM), which showed clear circular membrane vesicles with a diameter of ~90 nm (Figure 1B). We further quantified the number and size distribution of Y-exo and O-exo by NTA. The NTA showed a strong enrichment in particles in the range of 40–120 nm (Figure 1C). Interestingly, O-exo had a larger diameter (107 ± 0.8 nm, mean ± SE) relative to Y-exo (85 ± 0.7 nm) but were present at a lower concentration ($8.75 \pm 0.24 \times 10^{12}$ particles/mL, mean ± SEM) as compared to Y-exo ($1.44 \pm 0.42 \times 10^{13}$ particles/mL, mean ± SEM; Figure 1D) based on the same volume of serum, suggesting that the concentration and size of serum exosomes change with age.

Intravenously Injected Exosomes cross the Damaged BBB and Accumulate Mainly in the Penumbra after Ischemic Stroke.

Stroke occurs most often in the elderly population, and stroke patient outcomes are highly influenced by age.[35] Thus, in this study, aged rats were used as a model of acute ischemic stroke. However, aged rodents have higher mortality after MCAO due to frailty, peripheral immunosuppression, and other comorbid diseases.[36] In addition, aged rodents have less flexible vessels and heavier visceral fat making much more difficult to perform MCAO as does in young animals. We thus employed a permanent dMCAO model in aged rats to reduce mortality, as the mortality rate in aged rats after dMCAO with bilateral CCA occlusion was very high (50–60%) as compared to dMCAO without bilateral CCA occlusion (~5 %). Therefore, dMCAO without bilateral CCA occlusion was applied in young and aged rats in all experiments. Aged rat exhibited greater infarct volume and worse sensorimotor deficits as compared to young rats after dMCAO (Figure 1E and F).

The brain is traditionally considered an “immune-privileged” site due to the isolating effect of the blood-brain barrier (BBB),[37] which is, however, damaged after ischemic stroke. We intravenously injected 2% Evans Blue into aged rats 1 h or 23 h after ischemic stroke and sacrificed the rats 24 h after dMCAO. We found that Evans Blue predominantly accumulated in ischemic penumbra and infarct regions 1 h or 23 h after injection of Evans Blue (Online Figure I). The data confirm the BBB is disrupted after ischemic stroke.

To determine whether exosomes can delivery molecular signals from blood to brain, we labeled O-exo with a new proprietary, non-lipophilic dye for tracking exosome biodistribution *in vivo*. The labeled exosomes were intravenously administered into sham-operated and ischemic aged rats 3 h after dMCAO. Fluorescently labeled exosomes were observed in the most cells throughout the heathy and ischemic regions, including the striatum, hippocampus and cerebellum, 24 h after the injection, but were rarely detected in the subventricular zone (SVZ) (data not shown). Interestingly, the fluorescence signal intensity of labeled exosomes was much stronger in cells located in the penumbra of the cortex 24 h (Figure 1G) and reach the peak 72 h after dMCAO, compared with sham-operated control (Figure 1H). Since the fluorescence signal intensity could reflect the exosome concentration, our data suggest that serum exosomes preferably home to the cells in the penumbra after dMCAO. To determine how long the injected serum exosomes last in the brain, we injected fluorescently labeled exosomes into ischemic rats, and the rats

were euthanized at 3, 7, 14 and 21 days after injection. We found that fluorescently labeled exosomes could be observed in the brain cells until day 14, but barely detectable 21 days after injection. Stroke did not affect the brain distribution of exosomes up to 14 days after dMCAO. Moreover, using a laser scan confocal microscope, we identified the intracellular localization of labeled exosomes as the cellular cytoplasm. To determine the phenotypes of the labeled exosome-positive cells, immunofluorescence staining was performed on the brain sections using antibodies against GFAP (for astrocytes), NeuN (for neurons), Iba1 (for microglia) and vWF (for endothelial cells). As shown in Figure 1I, the labeled exosome-positive cells co-localized with NeuN, GFAP, Iba1 and vWF. These findings suggest that the intravenously injected serum exosomes can cross the BBB and be internalized by brain cells including neurons.

Y-exo Attenuate, and O-exo Deteriorate Stroke Outcome.

To determine whether peripheral circulating exosomes contributed to functional outcomes after ischemic stroke, Y-exo and O-exo were injected intravenously into aged rats 3 h after dMCAO, twice per day for 3 days (Figure 2A). The infarct volume was significantly reduced in the group treated with Y-exo, but was larger in the O-exo-treated group 72 h after injection, as compared to the vehicle-treated group (Figure 2B and C). Consistent with these results, the sensorimotor deficits assessed by ladder rung walking test were significantly improved in the Y-exo-treated aged rats and worsened in O-exo-treated rats as compared to the vehicle-treated animals (Figure 2D), supporting beneficial effects of Y-exo after stroke and O-exo treatment deteriorated the functional outcome in aged ischemic rats. By contrast, when O-exo were intravenously injected into young rats 3 h after dMCAO, twice per day for 3 days, no significant differences in the infarct volume and sensorimotor deficits were found, as compared to the vehicle-treated animals (Online Figure II). To determine the longer-term outcome after Y-exo treatment, sensorimotor and cognitive deficits were investigated at 3, 7, 14, 21 and 28 days after dMCAO. We found that sensorimotor deficits were improved in aged rats at 3 and 7 days after Y-exo treatment, compared with vehicle (Figure 2 E and F; Online Figure IIIA). Post-stroke cognitive impairment was attenuated 28 days in aged ischemic rats treated with Y-exo compared to vehicle (Online Figure IIIB and C). In addition, infarct volume was also reduced in aged ischemic rats 35 days after Y-exo treatment as compared to vehicle (Online Figure IIIE).

To determine clinical relevance of our approach, Y-exo was also injected 6 h after onset of ischemic stroke, the outcomes were evaluated 72 h after treatment. We found that the infarct volume was significantly reduced, and sensorimotor deficits were improved 72 h after Y-exo treatment, compared to vehicle (Figure 2G–I), suggesting that a wider therapeutic window may be applied to treat stroke patients in clinical setting.

Serum Exosome Priming of the Microglial Phagoptosis after Ischemic Stroke is Age Dependent.

Mounting evidence indicates that the microglia-mediated inflammatory response plays a fundamental role in the pathophysiology and prognosis after acute ischemic stroke. Activated microglia release both pro- and anti-inflammatory mediators, which display either detrimental or beneficial effects on neurons, respectively. In ischemic stroke, the

secondary damage occurs mainly in the ischemic penumbra, where neuronal cells are reversibly affected.[38] Therefore, the penumbra is a target for neurorepair and neuroprotective therapies.[39] Indeed, we found that the number of $Iba1^+$ microglia was substantially increased in the penumbra after dMCAO (Online Figure IVA). These microglia retracted their ramifications, displayed an amoeboid morphology (amoeboid microglia) and were immunopositive for CD68 (a lysosomal protein expressed at high levels by activated microglia and at low levels by resting microglia). Activated microglia were observed most frequently in the penumbra and to a minor extent in the infarct core 72 h after stroke. The number of microglia ($Iba1^+$) and activated microglia ($Iba1^+CD68^+$) in the ipsilateral cortex were increased compared to the contralateral cortex (Online Figure IVB). Western blot confirmed that the levels of Iba1 and CD68 were significantly increased in the penumbra after dMCAO (Online Figure IVC–F). Taken together, these findings indicate that after ischemic stroke, activated microglia accumulate primarily in the ischemic penumbra.

Intravenous injection of O-exo into aged rats 3 h after dMCAO resulted in a significant increase in $Iba1^+CD68^+$ activated microglia 72 h after treatment as compared to vehicle (Figure 3A and B). Most of these cells were distributed in the penumbral M1 region of the cerebral cortex (also called primary motor cortex), but only a few $Iba1^+CD68^+$ cells were found in the ischemic core. 72 h after ischemic stroke, aged rats treated with Y-exo exhibited significantly fewer $Iba1^+CD68^+$ cells in the penumbral M1 region of the parietal cortex than those treated with vehicle (Figure 3A and B). Few to no $Iba1^+CD68^+$ cells were found in the contralateral cortex (Online Figure IVB).

To investigate the link between microglial activation and phagoptosis, we performed triple-label immunofluorescence staining for Iba1, CD68 and Homer1 (a postsynaptic density protein and thus a marker for the synapse). The triple-immunopositive ($Iba1^+CD68^+Homer1^+$) microglia were observed in the penumbral M1 region of the cerebral cortex. Confocal images show that $Homer1^+$ puncta were localized inside the lysosome of $Iba1^+CD68^+$ microglia (Figure 3C). An increased frequency and higher density of $Homer1^+$ puncta in single microglia were found in the O-exo-treated aged ischemic brains (Figure 3C). Quantification of colocalized postsynaptic puncta revealed a significant loss of synapses in aged ischemic rats treated with O-exo, as compared to the vehicle group (Figure 3D). By contrast, ischemia-mediated loss of synapses in aged rats was significantly attenuated after intravenous injection of Y-exo 72 h after stroke (Figure 3D). These data indicate that O-exo significantly amplified the microglial phagoptosis in the penumbra after ischemic stroke.

After ischemic stroke, activated microglia polarize to the classic pro-inflammatory type (M1) or alternative protective type (M2). M1 microglia-mediated phagoptosis (primary phagocytosis) phagocytose live neurons or neurites and thus is detrimental. While M2 microglia-mediated phagocytosis (second phagocytosis) remove damaged/apoptotic cells and cell debris and are beneficial. Therefore, the beneficial or detrimental effects of activated microglia on neurons may be accounted for by their polarization state and functional responses after stroke. To examine the polarization of activated microglia in the ischemic brain after serum exosome treatment, immunofluorescence staining was performed using antibodies against M1-associated (CD86) and M2-associated (CD206)

proteins. Both Iba1^{+}CD86^{+} microglia (M1) and Iba1^{+}CD206^{+} microglia (M2) were observed in the penumbra after stroke (Figure 3E and G). Quantitative analysis showed that Iba1^{+}CD86^{+} microglia were significantly increased but Iba1^{+}CD206^{+} cells were reduced in the penumbral M1 regions in aged ischemic rats treated with O-exo as compared to vehicle (Figure 3F and H). The number of M1 and M2 microglia were altered, but not significantly, in the penumbral M1 regions in the aged ischemic rats 72 h after Y-exo treatment as compared to vehicle (Figure 3F and H).

The Effect of Serum Exosomes on Synaptic Plasticity is Age Dependent.

Based on the findings that O-exo exacerbated but Y-exo attenuated microglial phagocytosis of synapse as described above, we postulated that the effects of serum exosomes on synaptic function and plasticity in the ischemic brain are age dependent. The dendritic spines are the postsynaptic terminals that mediate synaptic transmission and plasticity.[40] Excitotoxicity is a key mechanism of neuronal injury in the ischemic brain associated with sensorimotor and cognitive deficits. We therefore investigated the effects of Y-exo and O-exo on ischemia-induced structural alterations in neuronal dendrites and dendritic spines in aged ischemic brain using Golgi-Cox staining (Figure 4A).

In these tests, cortical pyramidal neurons in layers II/III and V were analyzed in the penumbral M1 region of the ipsilateral cortex. The morphology of pyramidal neurons in three dimensions was reconstructed and dendritic spines were analyzed using Imaris software (Figure 4B and Online Figure VA). Although aging did not affect the average dendritic and spine length, the total dendritic length, segments and branches, the total length and number of dendritic spines were significantly reduced with age (Online Figure VC–E). We further confirmed that focal ischemia significantly decreased the total dendritic length and total dendritic spine length in surviving neurons. The spine density also dropped in the penumbral M1 region 72 h after dMCAO as compared to the corresponding contralateral cortex (Figure 4C–H).

The stroke-induced neuronal damage and loss of primary dendritic spines in the cortical penumbra were exacerbated by O-exo treatment as compared to vehicle. Conversely, Y-exo treatment ameliorated the destructive effects of focal ischemia on dendritic spine damage (Figure 4G–H). However, the mean lengths of individual spines and dendrites were similar across treatment groups (Online Figure VB).

To investigate the effects of Y-exo and O-exo on excitatory synaptic function, short-term plasticity and the probability of neurotransmitter release in the cortical penumbra after dMCAO, an experimental protocol of pair-pulse electrical stimulation in acute cortical brain slices was used. In these experiments, aged rats were randomly assigned to 3 groups (Y-exo, O-exo and vehicle) and subjected to dMCAO followed by the corresponding daily treatments for 72 h. The animals were then euthanized 72 h after dMCAO for preparation of acute cortical slices. Layer III cortical neurons located within ~500 μm from the ischemic core were identified by infrared imaging and used for patch-clamp electrophysiological recordings. To elicit evoked excitatory postsynaptic currents (ePSCs), a concentric stimulation electrode was position in the layer I and 50 pairs of identical brief electrical stimuli (~0.4 ms, ~0.8 mA) with a 250 ms of inter-stimuli interval (ISI)

were applied one pair every 15 seconds. Neurons in the penumbra across groups did not show significant differences in the resting potential measured in current-clamp: (p=0.1661, Kruskal-Wallis test, H=3.590; 2-tailed, unpaired). A Dunn's post-test multiple comparison test determined statistically insignificant (p<0.05) differences across groups: −64.8 mV (vehicle) vs. −60.3 mV (Y-exo) vs. – 60.8 mV (O-exo) (Figure 4I). By contrast, a strong distinct variability in the ratios of ePSC amplitudes (ePSC1/ePSC2) was detected across groups (Figure 4J–K). In these tests, the recorded neurons were held in voltage-clamp near −70 mV thus, near the neuronal resting potential and the reversal potential for GABAergic currents. The amplitude ratios showed significant differences across groups (p=0.0038, Kruskal-Wallis test, H=11.08; 2-tailed, unpaired). A Dunn's post-test multiple comparison test determined the following differences across groups: p<0.05, control vs. Y-exo; p<0.01, Y-exo vs. O-exo; and p>0.05; vehicle vs. O-exo. In total, 63 neurons in 26 cortical brain slices obtained from 10 aged ischemic rats were used in electrophysiological tests: 3 vehicle-injected, 4 Y-exo-injected and 3 O-exo-injected rats. To determine how the inter-pulse interval (IPI) affected the amplitude ratio across groups, in some neurons a shorter IPI (100 ms) was also tested (not shown). The shorter IPI reduced the amplitude ratios of ePSCs in all groups by a similar factor (0.88 for vehicle vs. 0.83 for Y-exo vs. 0.9 for O-exo) supporting the pre-synaptic nature of this observation. These differences across groups were not statistically significant (p=0.8948, Kruskal-Wallis test, H=0.2223; two-tailed, unpaired). A Dunn's post-test multiple comparison test determined insignificant differences between all pairs of groups (p>0.05). These results are consistent with a more reliable penumbral excitatory synaptic function and thus, an improved sensorimotor neurotransmission further supporting beneficial effects of Y-exo on sensorimotor functions.

Microglial Depletion Improves Effects of O-exo on Synaptic and Sensorimotor Function after Ischemic Stroke in Aged Rats.

To further investigate whether O-exo amplified microglial phagoptosis and worsened synaptic function and plasticity, we first depleted the microglia in the brain using PLX3397, a small-molecule CSF-1R inhibitor. Microglia are the only type of immune cells in the central nervous system (CNS) that express CSF-1 under physiological conditions,[41] and the development and survival of microglia critically depend on CSF-1R signaling.[42, 43] Administration of CSF-1R inhibitor can thus effectively wipe out microglia without harmful effects on other brain tissues.[42, 44] The aged rats were fed with PLX3397-containing chow or standard chow for 28 days and continued until the end of experiments to avoid the subsequent repopulation of microglia in the brain. The efficacy of microglial elimination by PLX3397 was determined based on immunofluorescence staining using anti-Iba1 (Figure 5A). The number of $Iba1^+$ cells in the cortex and striatum was significantly reduced in rats fed with the PLX3397-containing chow as compared with rats those on a standard chow (Figure 5B).

Next, we determined the level of microglial phagoptosis in these microglia-depleted aged ischemic brains 72 h after O-exo treatment. After depletion of microglia, the fluorescent signals corresponding to Homer1 expression in the lysosome of $Iba1^+CD68^+$ cells were significantly reduced (Figure 5C). Quantitative analysis showed that the number of $Iba1^+CD68^+$ cells in the penumbral M1 region was significantly reduced compared to

vehicle (Figure 5D), which was consistent with the reduction of triple^{+} puncta in each cell (Figure 5D). Dendritic and spines morphology after microglial depletion were also analyzed using the Imaris software. Aged ischemic rats with depleted microglia treated with O-exo showed a significant increase in the total length of dendrites and spines (Figure 5E–F) and number of dendritic and spine segments and branches (Figure 5E–F), as compared to O-exo treated rats with preserved microglia. These data indicate that in the ischemic brain, O-exo treatment alters synaptic morphology and amplifies microglial phagoptosis.

We then examined the effect of O-exo treatment on functional outcomes in aged ischemic rats fed a PLX3397-containing diet or a standard diet. Treatment with O-exo + PLX3397 significantly reduced brain injury and improved motor performance in ladder rung walking test (Figure 5 G and H) as compared to treatment with O-exo alone. Taken together, these results suggest that O-exo exerts harmful effects on synaptic organization and sensorimotor function by amplifying microglial phagoptosis. To determine the involvement of peripheral immune cells, immunostaining with antibodies against myeloperoxidase (MPO), CD11b and CD45 was performed. The number of CD11b^{+}CD45^{+} monocytes in the penumbra of O-exo-treated aged ischemic rats were significantly reduced by microglial depletion (Figure 5I). To further investigate the involvement of systemic inflammation, the levels of 27 cytokines and chemokines in serum of aged ischemic stroke treated with Y-exo or O-exo were measured using the Rat Cytokine Array/Chemokine Array. The levels of cytokines and chemokines in serum of aged ischemic rats were not significantly altered by Y-exo or O-exo treatments as compared to the vehicle group (Online Table I).

Proteomic Analysis Reveals Different Profiles of Complement Activity in Y-exo and O-exo.

To further investigate the mechanism underlying the deteriorating or beneficial effects of serum exosomes in ischemic rats, we analyzed the protein profiles of Y-exo and O-exo using proteomics. The Y-exo vs. O-exo protein profiles were defined as significantly different ($p<0.05$) if at least 1.5-fold change was detected with at least 2 unique peptides present. Among 277 proteins identified, 126 were significantly different between Y-exo and O-exo: 71 were up-regulated and 55 were down-regulated. Among these, 48 (38.1%) and 45 (35.7%) proteins were expressed only in Y-exo and O-exo, respectively (Figure 6A). A volcano plot shows these differentially expressed proteins according to their fold changes and *p*-values (Figure 6B). A biological heat map of clusters from the two groups was constructed using normalized data to provide an overview of the distribution of the expressed exosome proteins. After unsupervised hierarchical clustering, the heat map illustrated an overall reproducibility as well as individual heterogeneity of protein expression profiles among different subjects within Y-exo and O-exo (Figure 6C). The expression of complement proteins was 10-folds greater in O-exo compared to Y-exo. The identified differential proteins included C4b-binding protein (C4BP) α chain and β chain, CD59, plasma protease C1 inhibitor, C1q, complement factor I, complement factor H, and C3.

Next, we performed gene ontology (GO) enrichment analysis of the identified differentially expressed proteins to gain insight into the molecular functions and biological processes that might implicate ischemic outcome after serum exosome treatment. We found that differentially expressed proteins in Y-exo and O-exo were significantly enriched with

GO categories linked to protein processing regulation, humoral immune response, protein activation cascade, intracellular signal transduction, complement activation, cell recognition, protein processing and maturation regulation, acute inflammatory response regulation and phagocytic recognition and engulfment (Figure 6D).

We then verified the differential abundance of three selected complement proteins (CD46, C3a and C3b) in serum exosomes using Western blot (Figure 6E). Consistent with the trend found by the proteomics analysis, the Western blot results showed similar alterations in independent subsets of samples. The levels of CD46 proteins were significantly higher in Y-exo as compared to O-exo. Conversely, the relative intensities of C3a and C3b were higher in O-exo *vs.* Y-exo (Figure 6F).

To determine the timing and expression levels of C3aR and C3a/C3b on microglia, aged ischemic rats were injected with Y-exo or O-exo and $C3aR^{+}Iba1^{+}$ and $C3^{+}Iba1^{+}$ cells in the ischemic penumbra were recorded 24, 48 and 72 h using a confocal laser scanning microscope. We found that the levels of C3 (C3a/b) and C3aR on the active microglia in the penumbra were dramatically increased 48 h and 72 h after O-xo injection, compared to the groups treated with Y-exo and vehicle (Online Figure VI). By Western blot analysis, we also found that C3a, C3b, C3aR and CD68 in the ipsilateral cortex were increased 24, 48 and 72h after O-exo injection, but reduced after Y-exo treatment, compared to vehicle (Online Figure VII). We also found that C1q was increased in aged rats after dMCAO, which could be attenuated after Y-exo treatment (data not shown). Similarly, the levels of CD86 proteins were slightly increased but CD46 and CD206 were significantly reduced in the ipsilateral cortex of aged ischemic rats 3 days after injection of O-exo (Online Figure VIII). The levels of CD86 were reduced in the ischemic brain of aged rats injected with Y-exo (Online Figure VIII). Thus, these data suggest that higher levels of activated complement molecules in O-exo may prime the microglial response after ischemic stroke worsening the stroke outcome.

C3a Receptor Blockage Reverses O-exo–mediated Hyperactivation of Microglial Phagoptosis and Improves Stroke Outcome.

As complement C3 acts on microglial C3aR altering microglial phagoptosis of synapse, we next sought to investigate the functional effects of C3aR inhibitor (C3aRI; SB290157) on aged ischemic rats treated with O-exo. The number of $CD68^{+}Iba1^{+}$ cells in the penumbra was reduced in rats treated with a combination of O-exo and C3aRI as compared to treatment with O-exo alone (Figure 7A and B). Consistent with these results, the $Iba1^{+}CD68^{+}Homer1^{+}$ cells in the penumbra were also reduced 72 h after O-exo + C3aRI treatment (Figure 7C), suggesting that phagocytic microglia were reduced after inhibiting C3aR activity. The same control animals injected with O-exo with standard diet were used in experiments utilizing PLX3397 and SB290157 treatments.

Next, the total dendritic length and total number of dendritic segments and branches within the cortical penumbra 72 h after ischemic stroke were evaluated and found significantly greater in animals treated with a combination of O-exo + C3aRI as compared to treatment with O-exo alone (Figure 7D). Similar results were obtained for the total spine length and

the total number of spine segments (Figure 7E). These data suggest that inhibition of C3aR activity attenuates synaptic damage after O-exo treatment.

Inhibition of C3aR activity was also found to significantly reduce ischemic volume and sensorimotor deficits in aged ischemic rats after O-exo treatment. Aged rats treated with O-exo + C3aRI exhibited significantly smaller infarct volumes, as compared with animals treated with O-exo alone (Figure 7F–G). In the ladder rung walking test, animals treated with O-exo + C3aRI exhibited significantly better motor performance as compared to animals treated with O-exo alone (Figure 7H). Taken together, these data suggest beneficial effects of inhibition of C3aR in aged ischemic rats and point to a complement-dependent mechanism.

DISCUSSION

Aging is associated with immune dysregulation characterized by high levels of circulating pro-inflammatory mediators, which may result from repeated microbial infections, injury or chronic inflammation. Systemic inflammatory mediators contribute to age-related cognitive decline and chronic diseases,[45] but their role in ischemic stroke remains unexplored. Here, we report that the levels of serum exosomal complement components (C1q, C3a and C3b) that are increased with age can cross the BBB to prime microglia and augment microglial phagoptosis of synapses. By comparing the effects of Y-exo *vs.* O-exo *vs.* vehicle injected in aged ischemic rats, we determined the mechanisms of complement-microglial interactions and revealed therapeutic benefits of Y-exo treatment for synaptic, sensorimotor and cognitive functions after acute ischemic stroke. By contrast, O-exo treatment caused deleterious effects, which were reversed by microglial depletion and blockage of C3aR. The findings are summarized in Figure 8. These results are consistent with poorer prognosis for elderly stroke patients as compared to younger patients.

The ischemic penumbra is functionally impaired, but potentially salvageable. Spontaneous recovery of sensorimotor function after stroke is thought to be mediated primarily through the reorganization and rewiring of the surviving penumbral brain circuits. Neuronal dendrites and dendritic spines receive and process most of the excitatory synaptic signaling. Given that dendritic spine turnover underlies rewiring during normal development and plasticity, the stroke-induced changes in synaptic structure and the number of dendrites and dendritic spines in the penumbra likely contribute to sensorimotor and cognitive deficits that occur after stroke. We found that O-exo-induced sensorimotor deficit were accompanied by a reduced number of dendrites and dendritic spines. By contrast, Y-exo treatment after ischemic stroke supported synaptic plasticity and significantly improved synaptic, sensorimotor and cognitive functions. The amount of exosomes per injection was determined based on previous studies that injection of 100 μg exosomes from mesenchymal stem cells (MSCs) or hypoxia-preconditioned MSCs ameliorate cognitive decline[46] and improved stroke outcome.[14] Our results suggest that exosome-induced changes in the penumbral neuronal and synaptic structure particularly, at the level of dendrites and dendritic spines, are prime contributors to sensorimotor deficits. With age, neuronal dendritic trees undergo progressive regression which are further exacerbated by ischemic stroke. Restoration of synaptic organization and function are critical for recovery

of sensorimotor and cognitive functions after ischemic stroke in aged animals. The effects of Y-exo and O-exo on excitatory synaptic function, short-term plasticity and the probability of neurotransmitter release in the cortical penumbra after dMCAO were studied using an experimental protocol of pair-pulse electrical stimulation in acute cortical brain slices. The results indicated that Y-exo treatment significantly increased the probability of release in excitatory synapses in the cortical penumbra thereby changing the activity profile of excitatory synapses towards increasing the neurotransmitter release probability as compared to aged ischemic rats injected with O-exo or vehicle. Boosting the probability of synaptic release in the ischemic penumbra may compensate for the loss of synaptic function in the injured synaptic network deprived of fully functional neurons and synapses yet, facing the same sensorimotor challenges. These effects of Y-exo on penumbral excitatory synapses are consistent with a more reliable sensorimotor neurotransmission further supporting beneficial effects of Y-exo on sensorimotor function.

Phagoptosis and release of inflammatory cytokines are the key functions of microglia that contribute to secondary brain injury after stroke. Thus, microglial activation plays a dual role: beneficial and detrimental. On the one hand, microglial activation is necessary for the removal of debris for tissue repair (secondary phagocytosis). On the other hand, microglia also phagocytose live neurons or neurites (phagoptosis, also called primary phagocytosis), leading to secondary brain injury. Specifically, in the early stages, ischemic stroke mainly activates penumbral pro-inflammatory microglia and microglial phagoptosis of synapses, which could be further primed by O-exo or attenuated by Y-exo, as $CD68^+$/$Homer1^+$ cells in the penumbra were significantly increased after O-exo treatment The CD68 and Iba1 are commonly used as markers for macrophages and microglia. It is possible that CD68 would preferentially identify blood born macrophages. Therefore, $CD68^+$ cells could also be direct blood-derived monocytes/macrophages. Interestingly, we found that $CD11b^+/CD45^+$ monocyte infiltration is low in aged ischemic rats treated with O-exo after microglia depletion, compared to the vehicle group. Our findings suggest that despite profound increases in $CD11b^+/CD45^+$ monocytes/macrophages in penumbra after dMCAO in aged rats treated with serum exosomes, the majority of $CD68^+$ cells in acutely ischemic regions are microglia in aged rats treated with serum exosomes. Consistently, we found that most $CD68^+$ cells in the penumbra displayed morphological characteristics of activated microglia, suggesting that these cells are actively phagocytic microglia. After microglial depletion, the extent of O-exo–mediated synaptic loss in the penumbra was significantly reduced consistent with improved sensorimotor functions. These data suggest that microglial activation and its facilitation by O-exo treatment are harmful in the early stage of stroke primarily due to the elevated damage to synaptic organization and loss of synaptic function. Interestingly, we also found that $Iba\text{-}1^+/CD68^-/Homer1^+$ cells, were increased after Y-exo treatment, suggesting possibility of normal microglial involvement in beneficial phagocytosis, not phagoptosis only, for improved functional outcome by Y-exo.

We then examined the protein profile of serum exosomes to identify the trigger(s) of microglial activation. The levels of complement opsonins (C1q) and anaphylatoxins (C3a and C3b) were increased by O-exo, whereas CD46 was increased by Y-exo. The complement system is essential for activation of innate immune response and plays a vital role in host defense and tissue homeostasis. Complement system is also an important

driver of inflammation, and thus unbalanced or uncontrolled activation of complement cascade can cause systemic inflammation, tissue damage and disease.[47] Studies have also documented that complement emerges as both a masterful regulator of neural synaptic plasticity and an instigator of brain injury after acute ischemic stroke worsening outcomes.[48] Therefore, excessive complement activation induced by O-exo is expected to damage synaptic, sensorimotor and cognitive functions. Importantly, complement is critical for microglial activation and phagocytosis, as the C3aR expressed on microglial surface are essential for microglial activation. Thus, it is not surprising that inhibition of C3aR activity attenuated the negative effects of O-exo in aged ischemic rats. We concluded that after ischemic stroke O-exo act as deliver vehicles for pro-inflammatory modulators, such as complement opsonins and anaphylatoxins, cross the BBB and trigger microglial activation via C3aR, which leads to neuronal and dendritic damage and, subsequently, exacerbated sensorimotor and cognitive deficits. CD46 exhibits a cofactor activity for inactivation of complement C3b and C4b,[49] and thus, beneficial effects of Y-exo may in part originate from Y-exo-induced augmentation of CD46 levels and subsequent inhibition of microglial activation mediated by complement signaling in the ischemic brain.

The BBB plays a critical role in regulating the trafficking of fluid, solutes and cells at the blood-brain interface and maintaining the homeostatic microenvironment of the healthy brain. Under pathological conditions, the BBB can be damaged, leading to the extravasation of blood components into the brain and neuronal damage. Studies have documented that exosomes from brain cells are able to cross the BBB and can serve as biomarkers of cognitive impairment in Alzheimer's disease[50–52] and brain injury.[53] Blood exosomes can also cross the BBB to target brain cells and have been used as a drug delivery vehicle[54–57]. Therefore, exosomes can cross the BBB in a bi-directional manner. As most cells can synthesize and release exosomes into the body fluid circulation, serum exosomes originate from all organs.[58] By NTA analysis, we found that the concentration and size of Y-exo were different from O-exo suggesting different sources of origin. For example, brain-derived serum exosomes are more likely in aged animals because the BBB of the aged brain is more likely to be damaged after stroke and the damage is likely to be more severe than in young animals. For that reason, brain-derived exosomes have been proposed as a biomarker for certain age-related neurodegenerative disorders. We confirmed that BBB was disrupted in the ischemic brain, predominantly in the ischemic core/penumbra. We also revealed that circulating exosomes could cross the BBB in healthy and ischemic brains. However, the intravenously injected serum exosomes primarily accumulated within the cells in the ischemic penumbra consistent with the leaky BBB after ischemic stroke. The serum exosomes were taken up by recipient brain cells including neurons and microglia, indicating that exosomes act as effective vehicles to deliver peripheral pro-inflammatory mediators and other biomolecules to the brain.

In summary, aging blood exosomes progressively accumulate peripheral pro-inflammatory mediators and deliver them to the brain to prime and excessively activate microglia via a C3aR-dependent mechanism. This process is facilitated by ischemic stroke resulting in synaptic damage, reduced synaptic function and elevated sensorimotor and cognitive deficits. By replacing aging exosomes with young exosomes, it is possible to reverse the decline of synaptic and neurological functions and deliver therapeutic benefits after stroke.

Thus, peripheral and central immune systems are engaged in a continuous crosstalk via complement-microglial interactions and its modulation may serve as a promising therapeutic tool in ischemic stroke and other age-related brain diseases.

Supplementary Material

Refer to Web version on PubMed Central for supplementary material.

ACKNOWLEDGEMENTS

We thank Dr. Nathalie Sumien and Mr. Benjamin Landon for neurobehavioral testing and Dr. Zhengyang Zhou and Dr. Kiran Chaudhari for help with statistical analysis.

SOURCE OF FUNDING

This work was supported by National Institute of Health (NIH) grant R21NS094859 and American Heart Association grant 18PRE34020126.

Nonstandard Abbreviations and Acronyms:

O-exo	serum exosomes from aged rats
Y-exo	serum exosomes from aged rats
dMCAO	distal middle cerebral artery occlusion
CCA	common carotid artery
MCA	middle cerebral artery
NTA	nanoparticle-tracking analysis
CV	Cresyl violet
EB	Evans Blue
TTC	2,3,5-triphenyltetrazolium chloride
ACSF	artificial cerebrospinal solution
vWF	Von Willebrand Factor
CSF1R	colony stimulating factor 1 receptor
BBB	blood-brain barrier
IPI	inter-pulse interval
C3aRI	C3a receptor inhibitor

REFERENCES

1. Tinetti ME, Speechley M, Ginter SF. Risk factors for falls among elderly persons living in the community. N Engl J Med. 1988;319:1701–1707 [PubMed: 3205267]

2. Villeda SA, Plambeck KE, Middeldorp J, Castellano JM, Mosher KI, Luo J, Smith LK, Bieri G, Lin K, Berdnik D, Wabl R, Udeochu J, Wheatley EG, Zou B, Simmons DA, Xie XS, Longo FM, Wyss-Coray T. Young blood reverses age-related impairments in cognitive function and synaptic plasticity in mice. Nat Med. 2014;20:659–663 [PubMed: 24793238]

3. Villeda SA, Luo J, Mosher KI, Zou B, Britschgi M, Bieri G, Stan TM, Fainberg N, Ding Z, Eggel A, Lucin KM, Czirr E, Park JS, Couillard-Despres S, Aigner L, Li G, Peskind ER, Kaye JA, Quinn JF, Galasko DR, Xie XS, Rando TA, Wyss-Coray T. The ageing systemic milieu negatively regulates neurogenesis and cognitive function. Nature. 2011;477:90–94 [PubMed: 21886162]

4. Conboy IM, Conboy MJ, Wagers AJ, Girma ER, Weissman IL, Rando TA. Rejuvenation of aged progenitor cells by exposure to a young systemic environment. Nature. 2005;433:760–764 [PubMed: 15716955]

5. Brack AS, Conboy MJ, Roy S, Lee M, Kuo CJ, Keller C, Rando TA. Increased wnt signaling during aging alters muscle stem cell fate and increases fibrosis. Science. 2007;317:807–810 [PubMed: 17690295]

6. Loffredo FS, Steinhauser ML, Jay SM, Gannon J, Pancoast JR, Yalamanchi P, Sinha M, Dall'Osso C, Khong D, Shadrach JL, Miller CM, Singer BS, Stewart A, Psychogios N, Gerszten RE, Hartigan AJ, Kim MJ, Serwold T, Wagers AJ, Lee RT. Growth differentiation factor 11 is a circulating factor that reverses age-related cardiac hypertrophy. Cell. 2013;153:828–839 [PubMed: 23663781]

7. Zomer A, Vendrig T, Hopmans ES, van Eijndhoven M, Middeldorp JM, Pegtel DM. Exosomes: Fit to deliver small rna. Commun Integr Biol. 2010;3:447–450 [PubMed: 21057637]

8. Wolf PThe nature and significance of platelet products in human plasma. Br J Haematol. 1967;13:269–288 [PubMed: 6025241]

9. Zhang Y, Kim MS, Jia B, Yan J, Zuniga-Hertz JP, Han C, Cai D. Hypothalamic stem cells control ageing speed partly through exosomal mirnas. Nature. 2017;548:52–57 [PubMed: 28746310]

10. Dorn GW 2nd. Micrornas in cardiac disease. Transl Res. 2011;157:226–235 [PubMed: 21420033]

11. Cortez MA, Bueso-Ramos C, Ferdin J, Lopez-Berestein G, Sood AK, Calin GA. Micrornas in body fluids--the mix of hormones and biomarkers. Nat Rev Clin Oncol. 2011;8:467–477 [PubMed: 21647195]

12. Ruckh JM, Zhao JW, Shadrach JL, van Wijngaarden P, Rao TN, Wagers AJ, Franklin RJ. Rejuvenation of regeneration in the aging central nervous system. Cell Stem Cell. 2012;10:96–103 [PubMed: 22226359]

13. Pusic AD, Kraig RP. Youth and environmental enrichment generate serum exosomes containing mir-219 that promote cns myelination. Glia. 2014;62:284–299 [PubMed: 24339157]

14. Xin H, Li Y, Cui Y, Yang JJ, Zhang ZG, Chopp M. Systemic administration of exosomes released from mesenchymal stromal cells promote functional recovery and neurovascular plasticity after stroke in rats. J Cereb Blood Flow Metab. 2013;33:1711–1715 [PubMed: 23963371]

15. Xin H, Katakowski M, Wang F, Qian JY, Liu XS, Ali MM, Buller B, Zhang ZG, Chopp M. Microrna cluster mir-17–92 cluster in exosomes enhance neuroplasticity and functional recovery after stroke in rats. Stroke. 2017;48:747–753 [PubMed: 28232590]

16. Fisher M, Feuerstein G, Howells DW, Hurn PD, Kent TA, Savitz SI, Lo EH, Group S. Update of the stroke therapy academic industry roundtable preclinical recommendations. Stroke. 2009;40:2244–2250 [PubMed: 19246690]

17. Won SJ, Xie L, Kim SH, Tang H, Wang Y, Mao X, Banwait S, Jin K. Influence of age on the response to fibroblast growth factor-2 treatment in a rat model of stroke. Brain Res. 2006;1123:237–244 [PubMed: 17064673]

18. Swanson RA, Morton MT, Tsao-Wu G, Savalos RA, Davidson C, Sharp FR. A semiautomated method for measuring brain infarct volume. J Cereb Blood Flow Metab. 1990;10:290–293 [PubMed: 1689322]

19. Tureyen K, Vemuganti R, Sailor KA, Dempsey RJ. Infarct volume quantification in mouse focal cerebral ischemia: A comparison of triphenyltetrazolium chloride and cresyl violet staining techniques. J Neurosci Methods. 2004;139:203–207 [PubMed: 15488233]

20. Risher WC, Ustunkaya T, Singh Alvarado J, Eroglu C. Rapid golgi analysis method for efficient and unbiased classification of dendritic spines. PLoS One. 2014;9:e107591 [PubMed: 25208214]

21. Bayram-Weston Z, Olsen E, Harrison DJ, Dunnett SB, Brooks SP. Optimising golgi-cox staining for use with perfusion-fixed brain tissue validated in the zq175 mouse model of huntington's disease. J Neurosci Methods. 2016;265:81–88 [PubMed: 26459195]
22. Paxinos G, Watson C. Paxino's and watson's the rat brain in stereotaxic coordinates. Amsterdam; Boston: Elsevier/AP, Academic Press is an imprint of Elsevier; 2014.
23. Brown CE, Li P, Boyd JD, Delaney KR, Murphy TH. Extensive turnover of dendritic spines and vascular remodeling in cortical tissues recovering from stroke. J Neurosci. 2007;27:4101–4109 [PubMed: 17428988]
24. Papadopoulos CM, Tsai SY, Cheatwood JL, Bollnow MR, Kolb BE, Schwab ME, Kartje GL. Dendritic plasticity in the adult rat following middle cerebral artery occlusion and nogo-a neutralization. Cereb Cortex. 2006;16:529–536 [PubMed: 16033928]
25. Wang X, Mao X, Xie L, Greenberg DA, Jin K. Involvement of notch1 signaling in neurogenesis in the subventricular zone of normal and ischemic rat brain in vivo. J Cereb Blood Flow Metab. 2009;29:1644–1654 [PubMed: 19536070]
26. Jin K, Minami M, Lan JQ, Mao XO, Batteur S, Simon RP, Greenberg DA. Neurogenesis in dentate subgranular zone and rostral subventricular zone after focal cerebral ischemia in the rat. Proc Natl Acad Sci U S A. 2001;98:4710–4715 [PubMed: 11296300]
27. Ames RS, Lee D, Foley JJ, Jurewicz AJ, Tornetta MA, Bautsch W, Settmacher B, Klos A, Erhard KF, Cousins RD, Sulpizio AC, Hieble JP, McCafferty G, Ward KW, Adams JL, Bondinell WE, Underwood DC, Osborn RR, Badger AM, Sarau HM. Identification of a selective nonpeptide antagonist of the anaphylatoxin c3a receptor that demonstrates antiinflammatory activity in animal models. J Immunol. 2001;166:6341–6348 [PubMed: 11342658]
28. Lian H, Litvinchuk A, Chiang ACA, Aithmitti N, Jankowsky JL, Zheng H. Astrocyte-microglia cross talk through complement activation modulates amyloid pathology in mouse models of alzheimer's disease. J Neurosci. 2016;36:577–589 [PubMed: 26758846]
29. Spangenberg EE, Lee RJ, Najafi AR, Rice RA, Elmore MRP, Blurton-Jones M, West BL, Green KN. Eliminating microglia in alzheimer's mice prevents neuronal loss without modulating amyloid-beta pathology. Brain. 2016;139:1265–1281 [PubMed: 26921617]
30. Schaar KL, Brenneman MM, Savitz SI. Functional assessments in the rodent stroke model. Exp Transl Stroke Med. 2010;2:13 [PubMed: 20642841]
31. Metz GA, Whishaw IQ. Cortical and subcortical lesions impair skilled walking in the ladder rung walking test: A new task to evaluate fore- and hindlimb stepping, placing, and co-ordination. J Neurosci Methods. 2002;115:169–179 [PubMed: 11992668]
32. Gharbawie OA, Whishaw PA, Whishaw IQ. The topography of three-dimensional exploration: A new quantification of vertical and horizontal exploration, postural support, and exploratory bouts in the cylinder test. Behav Brain Res. 2004;151:125–135 [PubMed: 15084428]
33. Lenzlinger PM, Saatman KE, Hoover RC, Cheney JA, Bareyre FM, Raghupathi R, Arnold LD, McIntosh TK. Inhibition of vascular endothelial growth factor receptor (vegfr) signaling by bsf476921 attenuates regional cerebral edema following traumatic brain injury in rats. Restor Neurol Neurosci. 2004;22:73–79 [PubMed: 15272142]
34. Li W, Huang R, Shetty RA, Thangthaeng N, Liu R, Chen Z, Sumien N, Rutledge M, Dillon GH, Yuan F, Forster MJ, Simpkins JW, Yang SH. Transient focal cerebral ischemia induces long-term cognitive function deficit in an experimental ischemic stroke model. Neurobiol Dis. 2013;59:18–25 [PubMed: 23845275]
35. Chen RL, Balami JS, Esiri MM, Chen LK, Buchan AM. Ischemic stroke in the elderly: An overview of evidence. Nat Rev Neurol. 2010;6:256–265 [PubMed: 20368741]
36. Liu F, Yuan R, Benashski SE, McCullough LD. Changes in experimental stroke outcome across the life span. J Cereb Blood Flow Metab. 2009;29:792–802 [PubMed: 19223913]
37. Carson MJ, Doose JM, Melchior B, Schmid CD, Ploix CC. Cns immune privilege: Hiding in plain sight. Immunol Rev. 2006;213:48–65 [PubMed: 16972896]
38. Hossmann KA. Viability thresholds and the penumbra of focal ischemia. Ann Neurol. 1994;36:557–565 [PubMed: 7944288]
39. Ramos-Cabrer P, Campos F, Sobrino T, Castillo J. Targeting the ischemic penumbra. Stroke. 2011;42:S7–11 [PubMed: 21164112]

40. Hering H, Sheng M. Dendritic spines: Structure, dynamics and regulation. Nat Rev Neurosci. 2001;2:880–888 [PubMed: 11733795]
41. Waisman A, Ginhoux F, Greter M, Bruttger J. Homeostasis of microglia in the adult brain: Review of novel microglia depletion systems. Trends Immunol. 2015;36:625–636 [PubMed: 26431940]
42. Elmore MR, Najafi AR, Koike MA, Dagher NN, Spangenberg EE, Rice RA, Kitazawa M, Matusow B, Nguyen H, West BL, Green KN. Colony-stimulating factor 1 receptor signaling is necessary for microglia viability, unmasking a microglia progenitor cell in the adult brain. Neuron. 2014;82:380–397 [PubMed: 24742461]
43. Elmore MR, Lee RJ, West BL, Green KN. Characterizing newly repopulated microglia in the adult mouse: Impacts on animal behavior, cell morphology, and neuroinflammation. PLoS One. 2015;10:e0122912 [PubMed: 25849463]
44. Rice RA, Pham J, Lee RJ, Najafi AR, West BL, Green KN. Microglial repopulation resolves inflammation and promotes brain recovery after injury. Glia. 2017;65:931–944 [PubMed: 28251674]
45. Chung HY, Kim DH, Lee EK, Chung KW, Chung S, Lee B, Seo AY, Chung JH, Jung YS, Im E, Lee J, Kim ND, Choi YJ, Im DS, Yu BP. Redefining chronic inflammation in aging and age-related diseases: Proposal of the senoinflammation concept. Aging Dis. 2019;10:367–382 [PubMed: 31011483]
46. Cui GH, Wu J, Mou FF, Xie WH, Wang FB, Wang QL, Fang J, Xu YW, Dong YR, Liu JR, Guo HD. Exosomes derived from hypoxia-preconditioned mesenchymal stromal cells ameliorate cognitive decline by rescuing synaptic dysfunction and regulating inflammatory responses in app/ps1 mice. FASEB J. 2017
47. Morgan BP, Harris CL. Complement, a target for therapy in inflammatory and degenerative diseases. Nat Rev Drug Discov. 2015;14:857–877 [PubMed: 26493766]
48. Alawieh A, Langley EF, Tomlinson S. Targeted complement inhibition salvages stressed neurons and inhibits neuroinflammation after stroke in mice. Sci Transl Med. 2018;10
49. Riley-Vargas RC, Gill DB, Kemper C, Liszewski MK, Atkinson JP. Cd46: Expanding beyond complement regulation. Trends Immunol. 2004;25:496–503 [PubMed: 15324743]
50. Pulliam L, Sun B, Mustapic M, Chawla S, Kapogiannis D. Plasma neuronal exosomes serve as biomarkers of cognitive impairment in hiv infection and alzheimer's disease. J Neurovirol. 2019
51. Sun B, Dalvi P, Abadjian L, Tang N, Pulliam L. Blood neuron-derived exosomes as biomarkers of cognitive impairment in hiv. AIDS. 2017;31:F9–F17 [PubMed: 28692534]
52. Rani A, O'Shea A, Ianov L, Cohen RA, Woods AJ, Foster TC. Mirna in circulating microvesicles as biomarkers for age-related cognitive decline. Front Aging Neurosci. 2017;9:323 [PubMed: 29046635]
53. Gill J, Mustapic M, Diaz-Arrastia R, Lange R, Gulyani S, Diehl T, Motamedi V, Osier N, Stern RA, Kapogiannis D. Higher exosomal tau, amyloid-beta 42 and il-10 are associated with mild tbis and chronic symptoms in military personnel. Brain Inj. 2018;32:1277–1284 [PubMed: 29913077]
54. Alvarez-Erviti L, Seow Y, Yin H, Betts C, Lakhal S, Wood MJ. Delivery of sirna to the mouse brain by systemic injection of targeted exosomes. Nat Biotechnol. 2011;29:341–345 [PubMed: 21423189]
55. Matsumoto J, Stewart T, Banks WA, Zhang J. The transport mechanism of extracellular vesicles at the blood-brain barrier. Curr Pharm Des. 2017;23:6206–6214 [PubMed: 28914201]
56. Yang T, Martin P, Fogarty B, Brown A, Schurman K, Phipps R, Yin VP, Lockman P, Bai S. Exosome delivered anticancer drugs across the blood-brain barrier for brain cancer therapy in danio rerio. Pharm Res. 2015;32:2003–2014 [PubMed: 25609010]
57. Qu M, Lin Q, Huang L, Fu Y, Wang L, He S, Fu Y, Yang S, Zhang Z, Zhang L, Sun X. Dopamine-loaded blood exosomes targeted to brain for better treatment of parkinson's disease. J Control Release. 2018;287:156–166 [PubMed: 30165139]
58. Panteleev MA, Abaeva AA, Balandina ANet al.Extracellular vesicles of blood plasma: Content, origin, and properties. Biochemistry (Moscow), Supplement Series A: Membrane and Cell Biology volume2017;11:187–192

NOVELTY AND SIGNIFICANCE

What Is Known?

- Aging is associated with immune dysregulation characterized by high levels of circulating pro-inflammatory mediators.
- Systemic pro-inflammatory mediators contribute to age-related decline in functional integrity, but its contribution to ischemic stroke remains largely unknown.

What New Information Does This Article Contribute?

- Pro-inflammatory mediators in blood exosomes accumulate with age.
- Young and old blood exosomes cross the BBB and differentially affect stroke outcomes.
- Complement system in blood exosomes define stroke outcomes.
- Blood exosomes mediate their effects after stroke via microglial phagoptosis.
- Blood exosome-mediated synaptic plasticity is C3aR dependent.

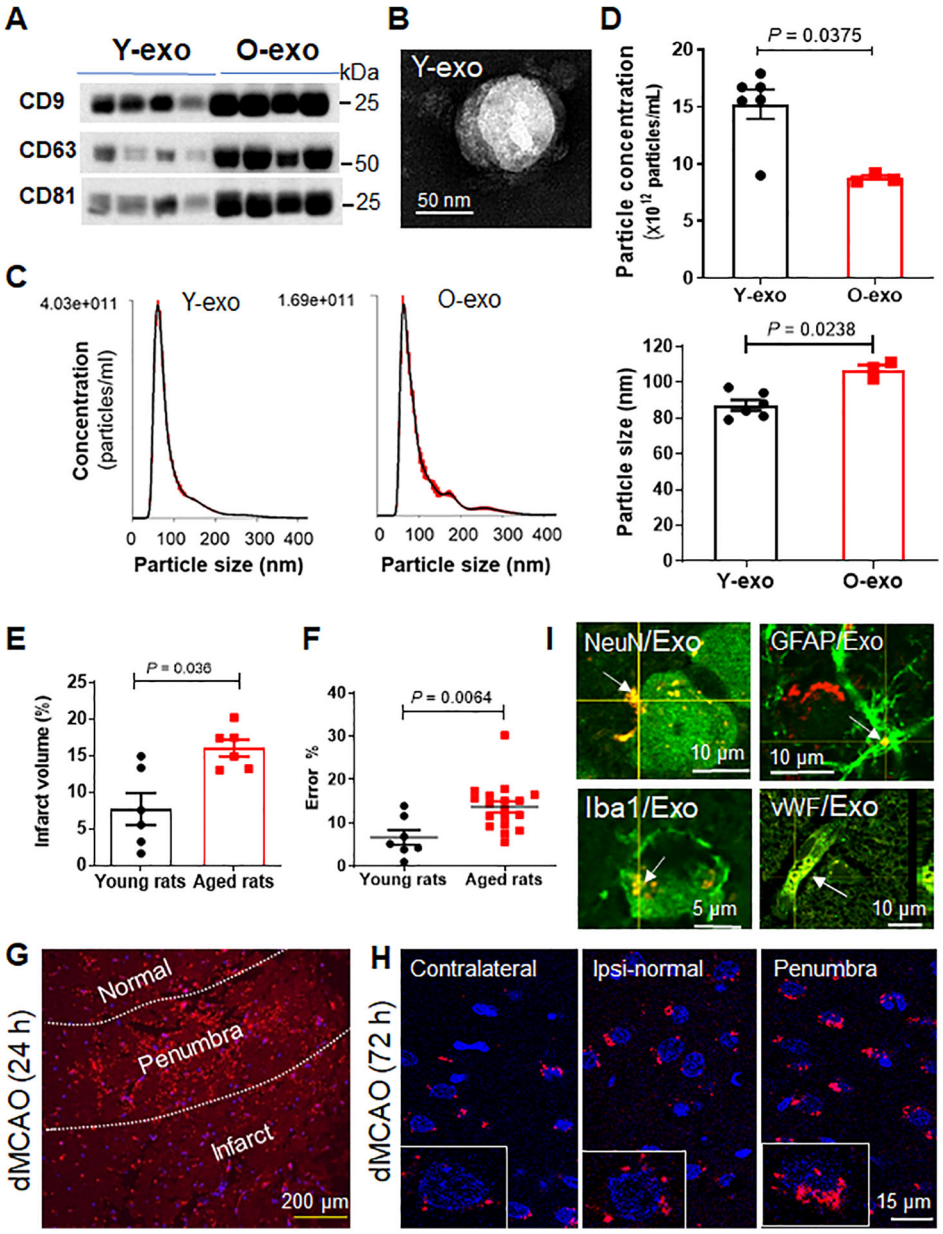

Figure 1. Serum exosome characterization with age, and evidence of peripheral circulating exosomes crossing the BBB.

A. Samples of serum exosomes obtained from young and aged rats were analyzed by Western blot with antibodies against exosome-specific markers CD9, CD63 and CD81. Experiments were repeated three times with similar results. **B**. A representative electron micrograph image showing typical morphology and size range of Y-exo. **C**. NTA was used to determine the concentration and size distribution of Y-exo and O-exo. **D**. Quantification of the concentration (top panel) and size (bottom panel) of serum exosomes determined by NTA. The sample size was N = 6 in the Y-exo group, and N = 3 in the O-exo group. The P values were assessed by a Mann-Whitney test. **E.** Quantitative analysis of infarct volume in young and aged rats 72 h after permanent dMCAO. The sample size is N = 6 per group. The P values were assessed by an unpaired Student's *t*-test. **F.** Sensorimotor deficits

assessed by the ladder rung walking test in young (N = 7) and aged (N = 18) rats 72 h after dMCAO. The P values were assessed by an unpaired Student's *t*-test. **G.** A representative image shows the distribution of fluorescently labeled exosomes (red) in the ipsilateral cortex 24 h after dMCAO. **H.** The pattern of fluorescently labeled exosome-positive cells (red) in the ischemic penumbra, ipsilateral normal cortex and contralateral cortex 72 h after dMCAO. DAPI was used as a nuclear counterstain (blue). Insert: higher magnification view of fluorescently labeled exosome-positive cells. **I.** Representative confocal microscopic images indicate that fluorescently labeled exosome-positive cells were positive for NeuN, GFAP, Iba1 and VWF expression in the ischemic cortex of aged rat. Data are presented as mean ± SEM. Exo, exosomes; Y-exo, serum exosomes from young rats; O-exo, serum exosomes from aged rats; Ipsi, ipsilateral.

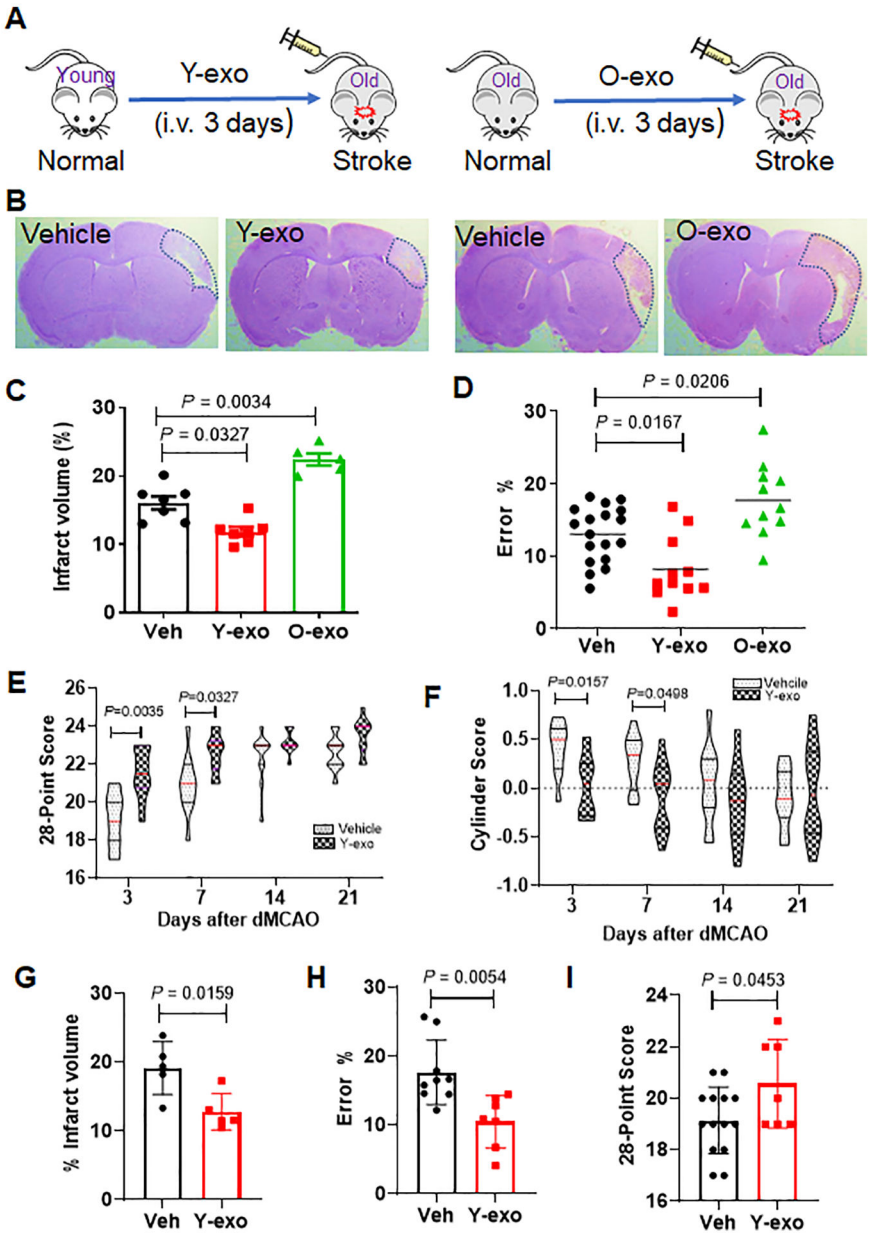

Figure 2. Effects of serum exosomes on stroke outcome are age-dependent.

A. Schematic illustration of intravenous injection of Y-exo (right panel) and O-exo (left panel) into aged ischemic rats 3 h after ischemic stroke, twice per day for 3 days. **B.** Representative images of CV-stained coronal brain sections of vehicle–, Y-exo– and O-exo–treated rats 72 h after focal ischemia. **C.** Quantitative analysis of infarct volume in vehicle–, Y-exo– or O-exo– treated rats 72 h after ischemic stroke. The sample size was N = 7 in the Veh and Y-exo groups, and N = 5 in the O-exo group. The P values were assessed by a one-way ANOVA followed by a Tukey's multiple comparisons test. **D.** Sensorimotor deficits of aged ischemic rats were assessed by the ladder rung walking test 72 h after administration of vehicle (N = 18), Y-exo (N = 11), or O-exo (N = 11). P values were shown and assessed by one-way ANOVA followed by Tukey's multiple comparisons test. **E-F.** The long-term

effect of Y-exo treatment on sensorimotor function assessed by 28-point neuroscore tests (E) and Cylinder test (F) 3, 7, 14 and 21 d after dMCAO (N = 11 per group). The P values were assessed by a 2-way repeated measures ANOVA with a Bonferroni post-hoc test. **G.** Delayed treatment (6 h after onset of ischemia) of Y-exo significantly decreased infarct volume in aged rats 72 h after dMCAO (N = 5 per group). The P values assessed by a Mann-Whitney test. **H** and **I.** The effect of delayed treatment of Y-exo on sensorimotor function assessed by the ladder rung walking test (H) and 28-point neuroscore tests (I). The sample size was N = 14 in the Veh group and N = 7 in the Y-exo group. Data are presented as the mean ± SEM. The P values were assessed by an unpaired Student's *t*-test. Y-exo, serum exosomes from young rats; O-exo, serum exosomes from aged rats. Dotted lines in B indicate the border of infarct core.

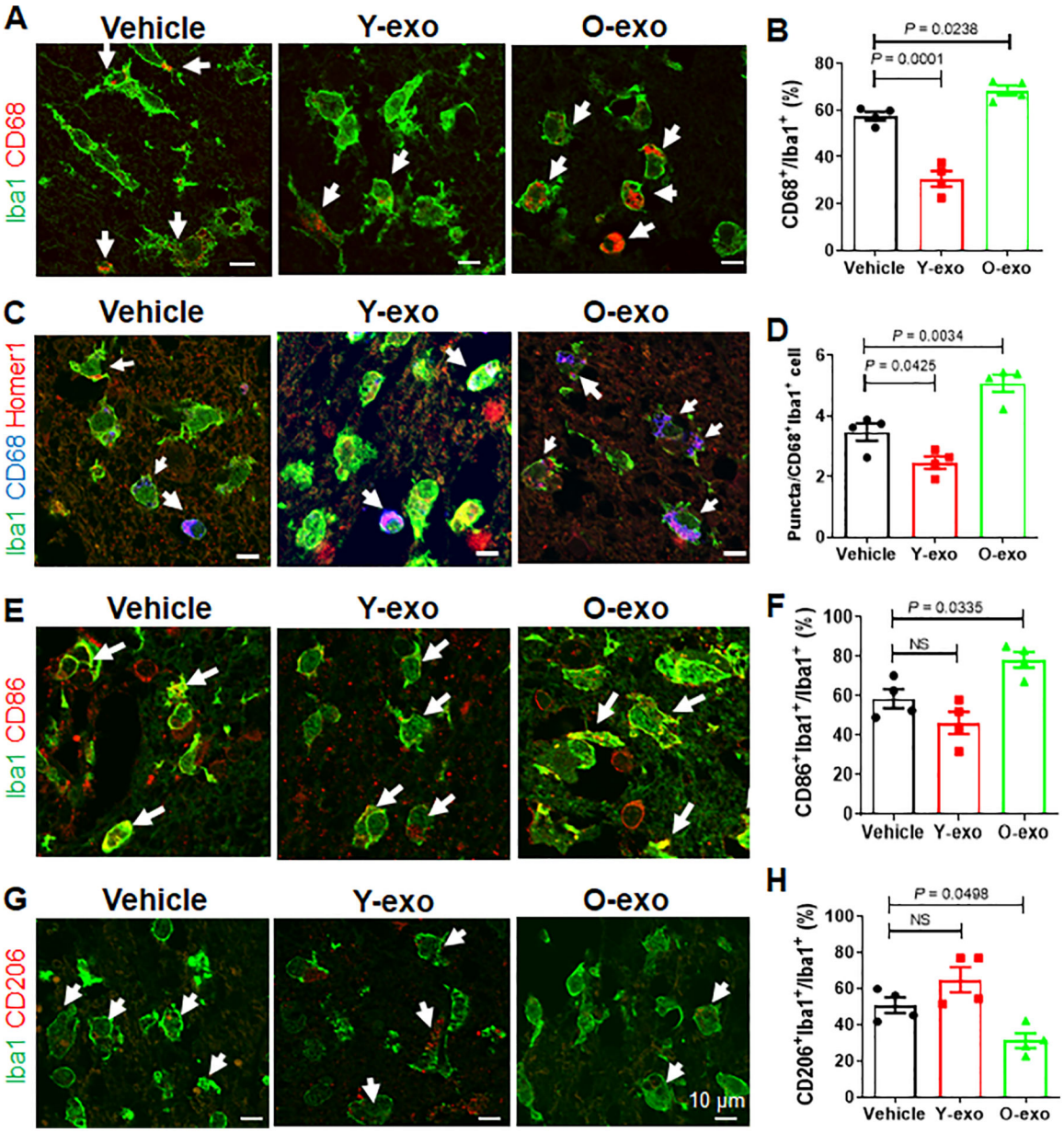

Figure 3. Serum exosomes prime the microglia response after ischemic stroke.

A. Representative confocal images of Iba1$^+$(green)CD68$^+$(red) microglia in the M1 region of the penumbra in aged ischemic rats treated with vehicle, Y-exo or O-exo. White arrows indicate Iba1$^+$CD68$^+$ microglia. **B.** Quantitative analysis of Iba1$^+$CD68$^+$ microglia in the penumbra in vehicle-, Y-exo– and O-exo–treated aged rats 72 h after dMCAO. **C.** Representative confocal images of Iba1$^+$ (green), CD68$^+$ (blue) and Homer1$^+$ (red) microglia in the penumbra after vehicle, Y-exo or O-exo treatment. **D.** Quantification of the phagocytic response of microglia in the M1 region of the penumbra in aged ischemic rats after vehicle, Y-exo or O-exo treatment. **E.** Representative confocal images from the penumbra (M1 region) showing expression of Iba1 (green) and CD86 (red) after serum exosome treatment. White arrows indicate Iba1$^+$CD86$^+$ microglia. **F.**

Quantification of Iba1^{+}CD86^{+} microglia in vehicle-, Y-exo– or O-exo–treated ischemic rats. **G.** Representative confocal images of Iba1 (green) and CD206 (red) in the penumbra of the aged ischemic brain after serum exosome treatment. White arrows indicate Iba1^{+}CD206^{+} microglia. **H.** The number of CD206^{+} microglia in the penumbra after vehicle, Y-exo or O-exo treatment. Each data point in the bar plots represents a biological replicate. Data are presented as the mean ± SEM. The P values were assessed by a one-way ANOVA with a Dunnett's post-hoc test in all panels. NS stands for not significant. Y-exo, serum exosomes from young rats; O-exo, serum exosomes from aged rats.

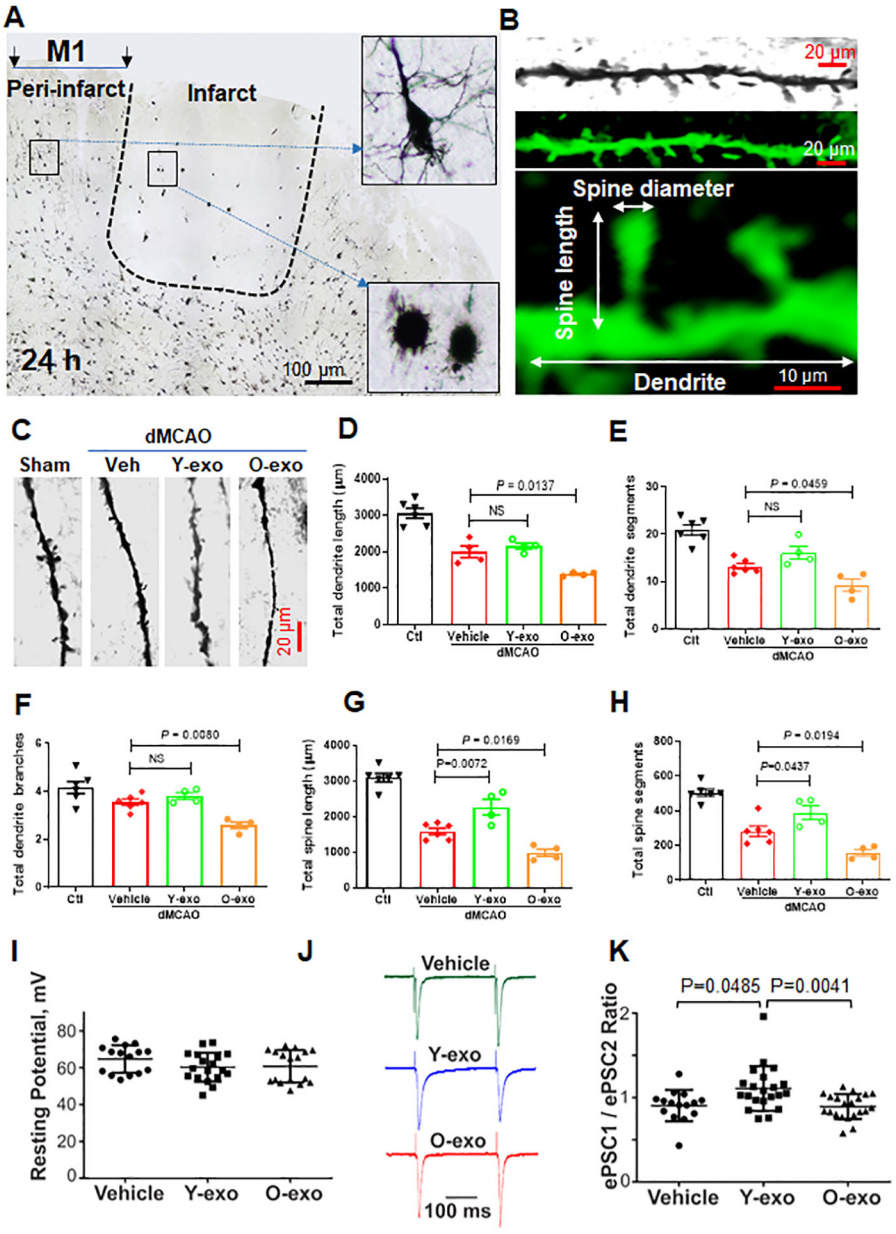

Figure 4. Serum exosomes contribute to synaptic organization and function in the aged ischemic brain.

A. Representative micrograph showing the pattern of Golgi-stained neurons from an aged ischemic brain. Insets show higher-magnification images of dendritic morphology of Golgi-Cox–stained cortical layer V pyramidal neurons from the penumbra and infarct core in the aged ischemic rat. **B.** Confocal images of a pyramidal neuron dendrite covered with spine segments. Top panel: cropped and enlarged image of Golgi-Cox–stained dendrite and spine segment. Middle panel: computer rendering of a dendritic segment with spines using Imaris software. Bottom panel: illustration of the structure of a neuronal dendrite and its spines. **C.** Representative high-magnification images of dendrite and spine segments of each group as indicated. **D–H.** Quantitative analysis of the effects of vehicle or serum exosomes on total dendritic length (D), total dendritic segments (E), total dendritic branches (F), total spine

length (G) and total spine segments (H) acquired from layers II/III and V pyramidal neurons in the penumbral cortex and in the corresponding contralateral cortex (Ctl). Each data point represents a biological replicate. P values were assessed by a one-way ANOVA with a Dunnett's post-hoc test. **I.** Current-clamp recordings: Effects of vehicle, Y-exo and O-exo treatments on the resting potential of layers III cortical neurons in aged ischemic rats. **J.** Voltage-clamp recordings: A stimulation electrode was positioned in the layer I and 50 pairs of identical brief electrical stimuli (~0.4 ms, ~0.8 mA) with a 250 ms of inter-stimuli interval were applied one pair every 15 seconds. A strong distinct variability in the ratios of ePSC amplitudes (ePSC1/ePSC2) was detected across groups. In these tests, the recorded neurons were voltage-clamped near −70 mV thus, near the neuronal resting potential and the reversal potential for GABAergic currents. **K.** A summary of pair-pulse stimulation experiment in voltage-clamp: ePSC1/ePSC2 ratio in aged ischemic rats treated with vehicle, Y-exo or O-exo for 3 days. The error bars represent the median with interquartile range. Each data point represents a biological replicate. The data were analyzed by a Kruskal-Wallis test with a Dunn's post-hoc multiple comparison test. NS stands for not significant. Y-exo, serum exosomes from young rats; O-exo, serum exosomes from aged rats.

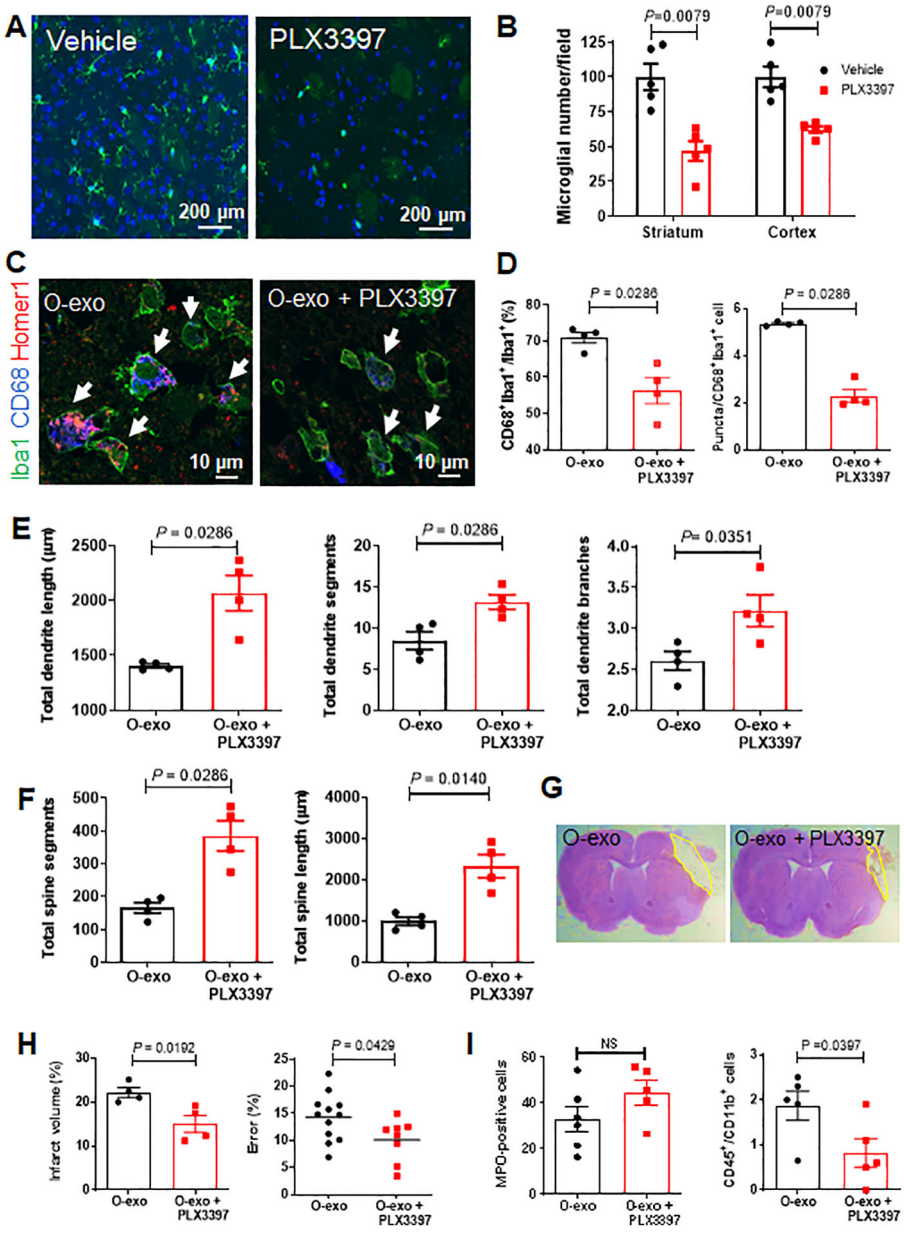

Figure 5. Microglial depletion reverses O-exo–mediated detrimental impairments in synaptic and sensorimotor function.

A. Representative images of brain sections from aged rats immunostained for Iba1 (green) after being fed a PLX3397-containing diet or a standard diet for 28 days. DAPI was used as a nuclear counterstain (blue). **B.** Quantitative analysis of $Iba1^+$ cells in the striatum and cortex of healthy aged rats treated with PLX3397 or vehicle (N = 5 per group). The P values were assessed by a Mann-Whitney tests. **C.** Representative confocal images of cells in the penumbral M1 region immunostained for Iba1 (green), CD68 (blue) and Homer1 (red) after treatment with O-exo alone or O-exo + PLX3397 for 3 days. White arrows indicate $Iba1^+CD68^+Homer1^+$ microglia. **D.** Quantitative analysis of $Iba1^+CD68^+$ cells (left panel) and the number of puncta in each activated microglia (right panel) in the penumbra of aged ischemic rats treated with O-exo alone or O-exo + PLX3397 for 3 days (N = 4 per group).

The P values were assessed by a Mann-Whitney test. **E** and **F.** Quantitative analysis of the effects of O-exo on total dendritic length (E), branches and segments and total spine length and segments (F) in aged ischemic rats fed a PLX3397-containing diet or a standard diet. N = 4 per group. P values were shown and assessed by Mann-Whitney tests for all panels in E and F. **G.** Representative images of CV–stained brain sections of aged ischemic rats treated with O-exo alone or O-exo + PLX3397 for 3 days. **H.** Quantification of infarct volume (left panel; N = 4 per group) and sensorimotor deficits (ladder rung walking test; right panel; N = 12 in the O-exo group and N = 8 in the O-exo + PLX3397 group) in aged ischemic rats fed a PLX3397-containing diet or a standard diet at 3 days after treatment with O-exo. The infarct volume was analyzed by a Mann-Whitney test. The sensorimotor deficits were analyzed by an unpaired Student's *t*-test. **I.** Quantitative analysis of MPO^+ cells (left panel) at 20× magnification and $CD45^+CD11b^+$ monocytes (right panel) in the penumbral M1 regions of aged ischemic rats fed a PLX3397-containing diet or a standard diet followed O-exo treatment. The data are shown as mean ± SEM (N = 5 per group). The P values were assessed by a Mann-Whitney tests. NS stands for not significant. O-exo, serum exosomes from aged rats.

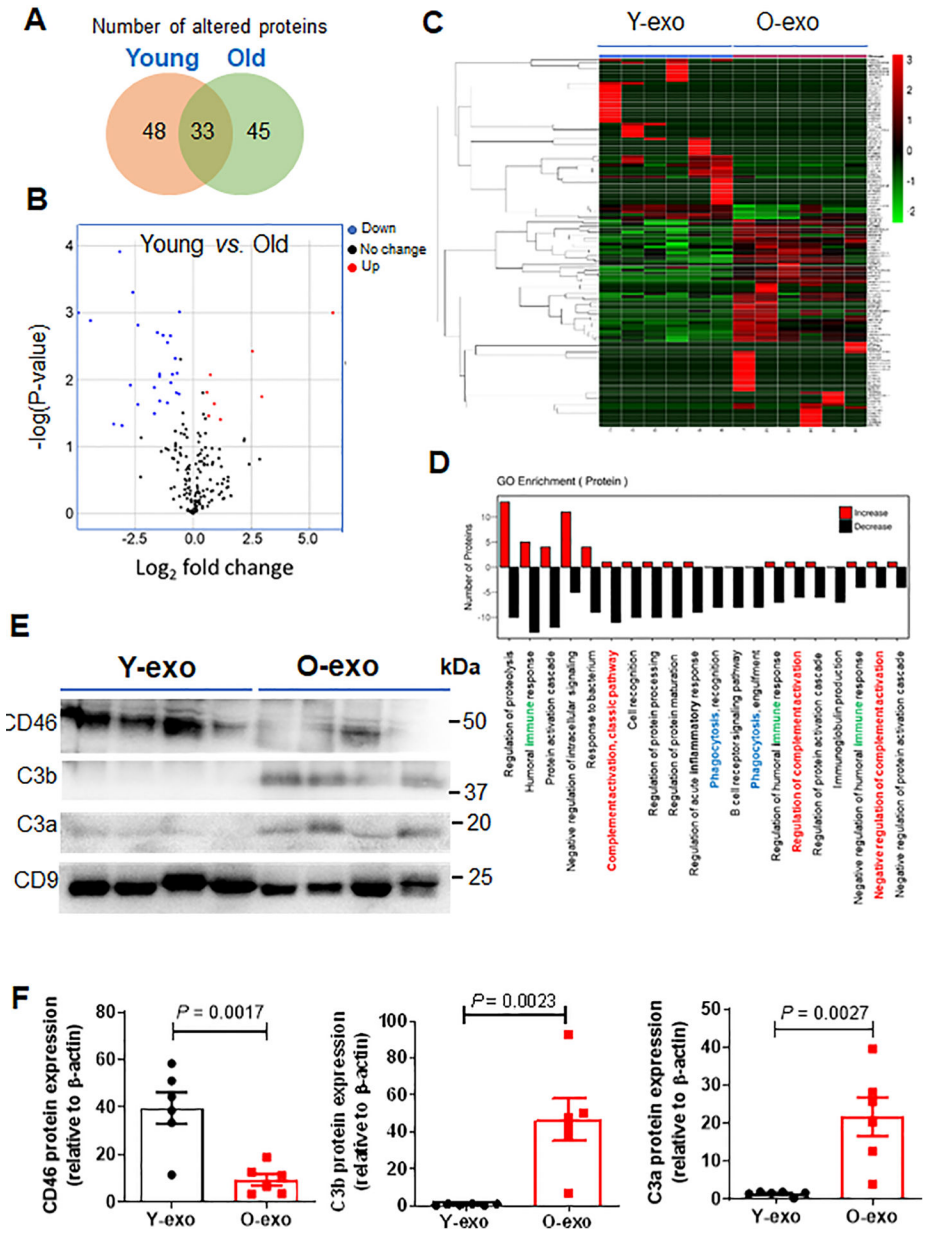

Figure 6. Proteomic profiles of Y-exo and O-exo.

A. Venn diagram depicts the overlap of the altered serum exosome proteins between normal young and aged rats as determined by proteomics. A total of 126 proteins were significantly different between Y-exo and O-exo. Among these, 48 and 45 proteins were expressed only in Y-exo and O-exo, respectively. **B.** Volcano plot displaying the distribution of identified serum exosome protein changes with age and significance (N = 6 per group). The data were analyzed by a Fisher's exact test. **C.** Heatmap representation of significantly changed proteins. Fold change values > 1.5 and a *p*-value < 0.05 were set as the filter criteria (N = 6 per group). The data were analyzed by a Fisher's exact test. **D.** A GO enrichment analysis for biological processes of up-regulated (red) and down-regulated (black) proteins in Y-exo was performed. Immune, complement cascade and phagocytosis in the GO categories are

indicated by green, red and blue, respectively. **E.** Western blot analysis of Y-exo and O-exo using antibodies against CD46, C3b and C3a. C9 was used as a protein control for protein loading and normalization of protein levels. **F.** The expression levels of selected proteins detected by Western blot were normalized to the β-actin level of the same sample. Data represent the mean ± SEM (N = 6 biological replicates for the Y-exo and O-exo groups) using unpaired two-tailed Student's t-test. Each experiment was repeated three times with similar results. The data are shown as mean ± SEM. Y-exo, serum exosomes from young rats; O-exo, serum exosomes from aged rats.

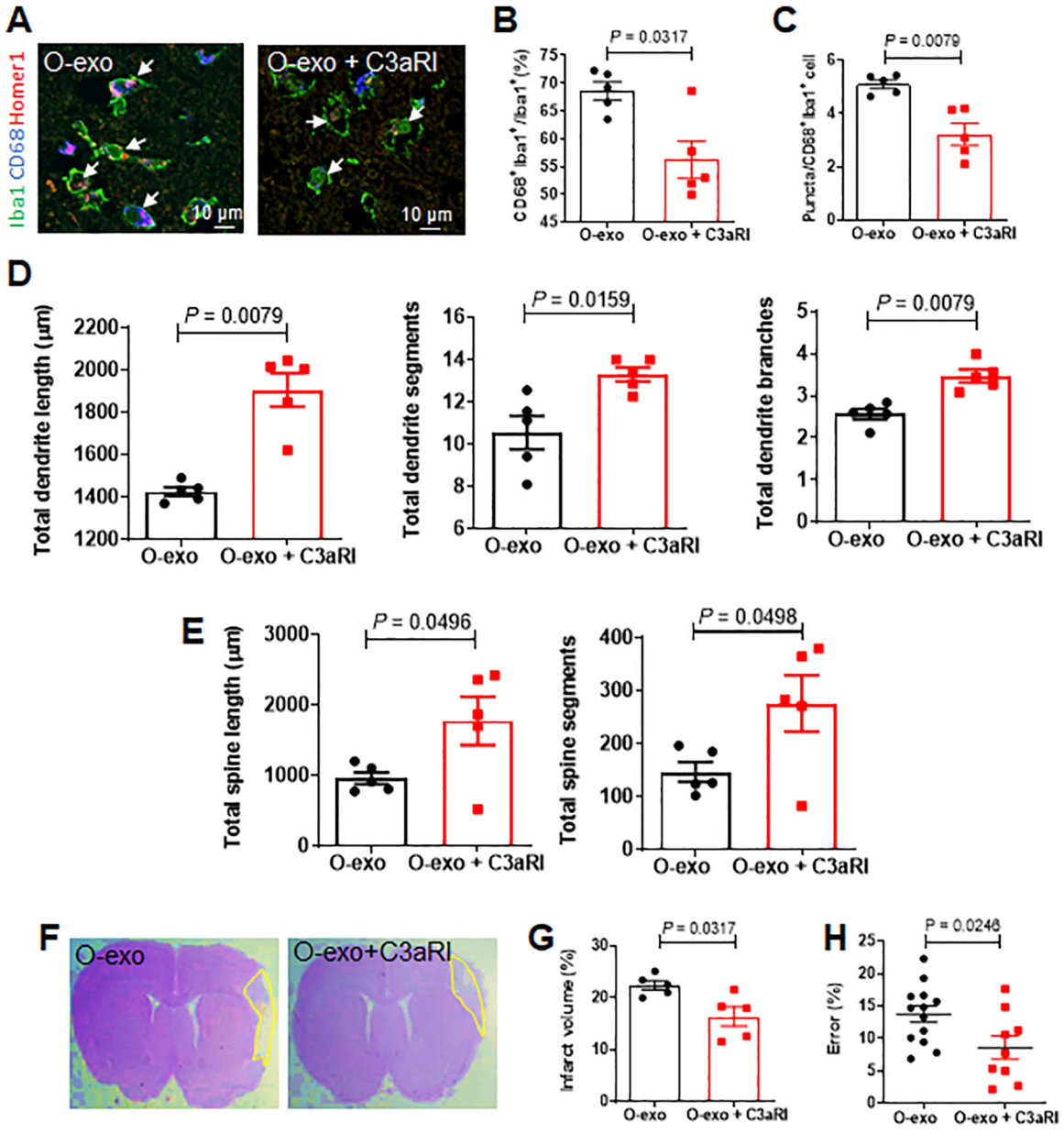

Figure 7. Inhibiting C3aR activity ameliorates O-exo–mediated detrimental effects in the aged ischemic brain.

A. Confocal images showing Iba1 (green), CD68 (blue) and Homer1 (red) expression in the penumbra in aged ischemic rats treated with O-exo or a combination of O-exo and C3aR inhibitor (C3aRI). White arrows indicate $Iba1^{+}CD68^{+}Homer1^{+}$ microglia. **B.** Quantification of $Iba1^{+}CD68^{+}$ activated microglia in aged ischemic rats 72 h after injection of O-exo with or without C3aRI (N = 5 per group). The P values were assessed by a Mann-Whitney test. **C.** Quantification of triple^{+} puncta per $Iba1^{+}$ cells in the aged ischemic brain after injection of O-exo with and without C3aRI (N = 5 per group). The P values were assessed by a Mann-Whitney test. **D**, **E.** Quantification of total dendritic length (D), segments and branches and total spine length and segments (E) in the penumbra of aged ischemic rats 72 h after O-exo injection with or without C3aRI (N = 5 per group). The P values were

assessed by a Mann-Whitney test. **F**. Representative CV-stained images showing infarct area in animals treated with O-exo alone or combination of O-exo and C3aRI. **G**. Infarct volume in aged ischemic rats treated with O-exo alone or combination of O-exo and C3aRI (N = 5 per group). The P values were assessed by a Mann-Whitney test. **H**. Sensorimotor deficits were determined by the ladder rung walking test in aged ischemic rats treated with O-exo alone or combination of O-exo and C3aRI. Data represent mean ± SEM. Each data point represents a biological replicate. The P values were assessed by unpaired Student's *t*-test. O-exo, serum exosomes from aged rats.

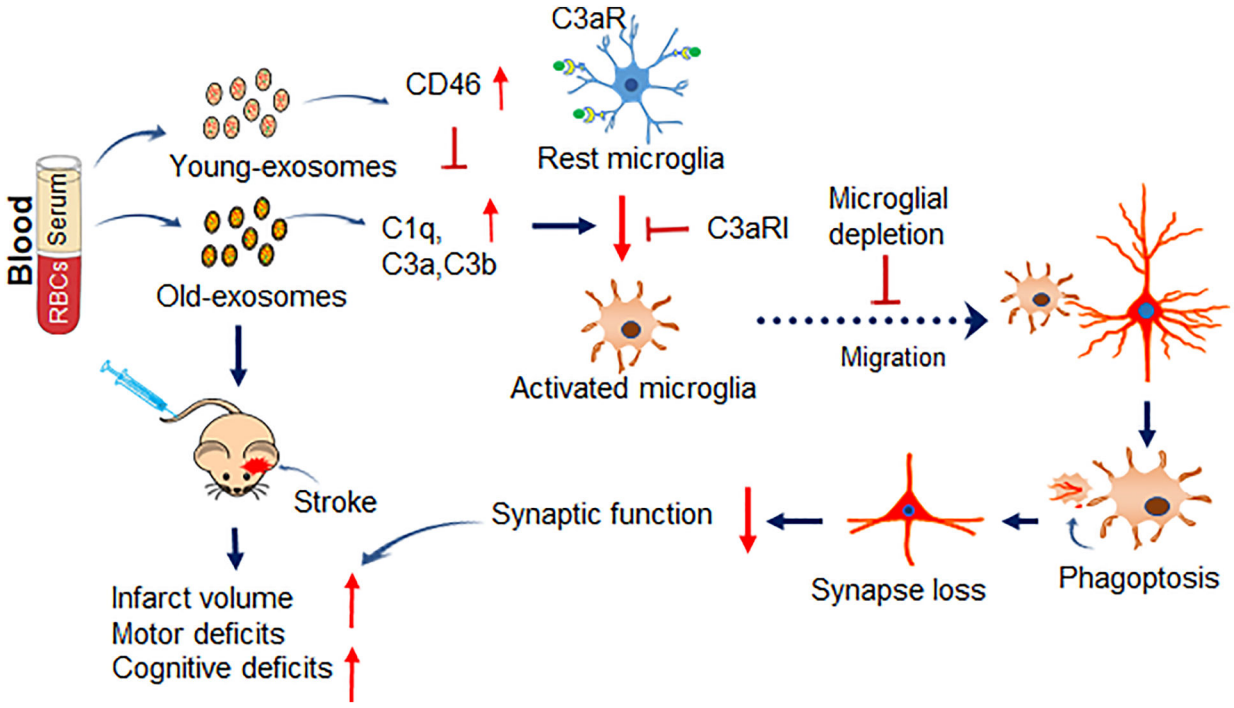

Figure 8. Illustration of Inflammatory blood exosomes affect stroke outcome by engaging the C3aR-dependent phagoptosis.

Complement opsonins and anaphylatoxins that accumulate in blood exosomes with age can prime microglia making them prone to excessive activation that exacerbates phagoptosis of synaptic damage and sensorimotor and cognitive deficits after ischemic stroke *via* microglial C3aR. In Y-exo, there is an increased level of CD46, which blocks complement cascade, and thus microglial activation, to attenuate negative ischemic outcomes. Y-exo, serum exosomes from young rats; O-exo, serum exosomes from aged rats; C3aRI, C3aR inhibitor.